



# CHORUS

This is the accepted manuscript made available via CHORUS. The article has been published as:

## Multicomponent hydrodynamic model for heterogeneous biofilms: Two-dimensional numerical simulations of growth and interaction with flows

Brandon Lindley, Qi Wang, and Tianyu Zhang

Phys. Rev. E **85**, 031908 — Published 9 March 2012

DOI: [10.1103/PhysRevE.85.031908](https://doi.org/10.1103/PhysRevE.85.031908)

**A Multicomponent Hydrodynamic Model for Heterogeneous Biofilms: 2-D  
Numerical Simulations of Growth and Interaction with Flows**

Brandon Lindley\*

*Code 6792, U.S. Naval Research Laboratory, Washington, DC 20375, USA*

Qi Wang

*Department of Mathematics, Interdisciplinary Mathematics Institute,  
and NanoCenter, University of South Carolina, Columbia, SC 29208, USA<sup>†</sup>*

Tianyu Zhang

*Department of Mathematical Sciences, Montana State University,  
P.O. Box 172400, Bozeman, MT 59717, USA*

## Abstract

We develop a tri-component (ternary) hydrodynamic model for multiphase flows of biomass and solvent mixtures, which we employ to simulate biofilm. In this new model, the three predominant effective components in biofilms, the extracellular polymeric substance (EPS) network, bacteria, and effective solvent (consisting of the solvent and nutrient, etc.), are modeled explicitly. The tri-component fluid mixture is assumed incompressible as a whole, while inter-component mixing, dissipation, and conversion are allowed among the effective components. Bacterial growth and EPS production due to the growing bacterial population are modeled in the biomass transport equations. Bacterial decay due to starvation and natural causes is accounted for in the bacterial population dynamics to capture the possible bacterial population reduction due to depletion of nutrient. In the growth regime for biofilms, the mixture behaves like a multiphase viscous fluid, in which the molecular relaxation is negligible in the corresponding time scale. In this regime, dynamics of biofilm growth in solvent (water) are simulated using a 2-D finite difference solver that we developed, in which distribution and evolution of EPS and bacterial volume fractions are investigated. The hydrodynamic interaction between the biomass and the solvent flow field is also simulated in a shear cell environment, demonstrating the spatially and temporally heterogeneous distribution of EPS and bacteria under shear. This model together with the numerical codes developed provides a new predictive tool for studying biomass-flow interaction and other important biochemical interactions in the biofilm and solvent fluid mixture.

---

\* Corresponding author e-mail: brandon.lindley.ctr@nrl.navy.mil

† Joint affiliation: School of Mathematics, Nankai University, Tianjin, P. R. China

## I. INTRODUCTION

Biofilms are common aggregates of microorganisms which form when cells adhere to surfaces in moist environments. These cells attach by excreting a slimy, glue-like substance called the extracellular polymeric substance (EPS) which encapsulates the bacteria colony and protects it from being washed away and attacked by foreign agents. Biofilms can be harmful or costly causes of medical implant contamination, airway, sinus and ear infections, tooth decay, periodontal disease, and industrial damage where they can contribute to metal fouling. The microbes within a biofilm are often much more resistant to antibacterial agents than planktonic cells of the same type, and thus pose a particular challenge to those interested in eradicating them. Despite their often pathogenic and destructive nature, biofilms can also be beneficial when utilized in mineral recovery, water purification or as bio-sealant to prevent leakage of gases.

The formation of bacterial biofilm involves a significant phenotypic shift as cells switch from the planktonic (free-swimming) to the surface-attached state. Within this attached colony, it is common that a biofilm contains differentiated cells, some of which behave distinctively under different chemical and environmental conditions. For instance, some of the bacteria are susceptible to antibacterial agents while others can develop a resistance by entering a transient dormant state where they are known as “persister cells.” Between these types of bacteria, complicated cellular processes can prompt a switch from one type into the other and vice versa [1]. In addition to the variety of bacterial cells, there exists a phenomenon called “quorum sensing” in which bacteria can regulate their production capability based upon the concentration of specific chemicals, called autoinducers, that each cell emits [2]. Experimental evidence shows that these chemical signals serve as a form of communication for bacteria cells, serving to recruit new members and regulate the growth of the colony.

Because of their heterogeneity and complexity, modeling biofilms has been a challenging task. A host of mathematical models have been proposed to model biofilm dynamics qualitatively. These include low dimensional models primarily focused on steady states [3–7], discrete-continuum models coupled with automata [8–18], continuum models for spatial heterogeneity [19, 20], multi-fluid models [19, 21–23], and our own one fluid multicomponent, binary phase field model [24–26]. For a detailed account of mathematical models of biofilm, please refer to our recent review article on the very subject [27] and an excellent, more recent, review by Klapper and Dockery [28]. Among all the models developed so far, very few have modeled the EPS network

separately from the bacterial population. However, microscopic imaging of biofilms clearly shows the distribution of bacteria and EPS network exhibits a highly heterogeneous microscopic structure [29]. This observation strongly suggests that these two species need to be modeled explicitly in any refined biofilm model. As mentioned, a few models do resolve the EPS network separately from the bacterial population [2, 30–33], yet none of these models are fully capable of resolving dynamic interactions between the EPS, bacteria, substrate and flow field.

In this paper, we propose a general framework for multicomponent materials that can handle dynamical interaction among multiple species and their inter-conversion, dissipation and mixing. In this formulation, the entire material system is approximated as incompressible. Thus, when the volume fraction of one species grows, the volume fraction(s) one or more of the others must be replaced by the growing species. We will adopt an incremental strategy in the systematic development of this biofilm model, focusing on the most basic features of biofilm formation here and adding more detail to the model in subsequent papers. Thus, we neglect the cellular communication effects related to quorum sensing and other molecular signaling pathways in this paper, but plan to address these issues in the future.

Our focus in this paper centers on developing detailed physical descriptions of the mechanistic behavior of various effective biofilm components, and the chemical kinetics involving the most basic ingredients. For multiphase materials, different species can have relative motion due to osmotic pressure and density stratification. We posit these relative motions are the result of non-equilibrium thermodynamical processes. Historically, a hydrodynamical theory for multiphase fluids can be formulated in two different ways. In one formulation, each phase is modeled explicitly using its own momentum and mass density. This approach ensures that the total mass and momentum are conserved. However, the velocity field for each individual phase has to be tracked in the entire material’s domain. Since these velocity fields are, in general, not measurable when an inflow-outflow boundary is present, it poses an insurmountable challenge on how to deal with this mathematically and physically [22]. The other formulation, the one fluid multicomponent approach, can handle this requirement naturally, and thus it is the approach we will use. In this formulation, the interpenetration or mixing among the various phases due to density stratification is modeled through an interaction potential. More specifically, the mixing or interpenetration is due to the “dynamic” osmotic pressure effect. In other words, mixing is regarded as a nonequilibrium thermodynamical process instead of a purely hydrodynamic one. The velocity for each individual phase can then be decomposed into the sum of a mean velocity (which resolves the bulk hydrodynamic interactions)

and an excessive velocity (which is due entirely to the nonequilibrium thermodynamics).

The rest of the paper is organized as follows. First, we briefly describe our ternary theory for biofilms, which involves treating EPS and bacteria as two distinct and yet interacting species explicitly. We then discuss the numerical scheme for the governing system of equations and, finally, we develop a new computational tool to simulate biofilm growth and interaction with surrounding solvent flows.

## II. MATHEMATICAL FORMULATION OF THE THREE COMPONENT MODEL FOR BIOFILMS

We briefly discuss the three-component model, also referred to as the ternary model in this paper, whose basic ingredients are developed in [34]. In this theory, we model the EPS and the bacteria as two interacting, yet distinct components, while the surrounding liquid and all dissolved nutrients and other materials are collectively modeled as an effective solvent. Since the total mass and volume of the nutrient in the biofilm are negligibly small, this mass and volume fraction are not normally modeled explicitly in theories for biofilms [35]. Hence, only the biochemical and diffusive effect of the nutrient is singled out and accounted for explicitly.

The structure and composition of a biofilm can vary widely depending upon the local environment and the types of bacteria which comprise it. Some biofilms behave primarily as viscoelastic solids, while others are best characterized as a heterogeneous complex fluid mixture [36]. Our focus is on biofilms which behave primarily as a complex fluid mixture. This type of biofilm is estimated to be 80% or more water, with most of this water stored within the bacterial cells which typically comprise 2-5% of the biofilm's biomass (though they can comprise more for certain densely packed biofilms). The rest of the biofilm's biomass is comprised of a 1-5% EPS solution (by volume fraction) [29, 37]. While planktonic bacteria at low to moderate concentrations are generally modeled as a suspension or collection of particles, the tightly packed bacteria typical of a biofilm should be regarded, along with the EPS matrix, as a bulk heterogeneous complex fluid [36], whose physical properties may depend on the density, size, shape and orientation of the individual bacterial cells.

In this model, we denote the volume fraction of the EPS network by  $\phi_n$ , that of the bacteria by  $\phi_b$ , and that of the solvent by  $\phi_s$ .

### A. Transport equations of the volume fractions

The transport of the volume fractions is governed by a system of modified or singular Cahn-Hilliard equations [38, 39] with reactive terms

$$\begin{aligned} \frac{\partial \phi_n}{\partial t} + \nabla \cdot (\phi_n \mathbf{v}) &= \nabla \cdot [\alpha_{11} \nabla (\frac{\delta f}{\delta \phi_n} - \frac{1}{2} (\frac{\delta f}{\delta \phi_b} + \frac{\delta f}{\delta \phi_s})) + \frac{1}{2} (\alpha_{22} - \alpha_{33}) \nabla (\frac{\delta f}{\delta \phi_s} - \frac{\delta f}{\delta \phi_b})] + g_n, \\ \frac{\partial \phi_b}{\partial t} + \nabla \cdot (\phi_b \mathbf{v}) &= \nabla \cdot [\alpha_{22} \nabla (\frac{\delta f}{\delta \phi_b} - \frac{1}{2} (\frac{\delta f}{\delta \phi_n} + \frac{\delta f}{\delta \phi_s})) + \frac{1}{2} (\alpha_{11} - \alpha_{33}) \nabla (\frac{\delta f}{\delta \phi_s} - \frac{\delta f}{\delta \phi_n})] + g_b, \end{aligned} \quad (\text{II.1})$$

$$\frac{\partial \phi_s}{\partial t} + \nabla \cdot (\phi_s \mathbf{v}) = \nabla \cdot [\alpha_{33} \nabla (\frac{\delta f}{\delta \phi_s} - \frac{1}{2} (\frac{\delta f}{\delta \phi_b} + \frac{\delta f}{\delta \phi_n})) + \frac{1}{2} (\alpha_{22} - \alpha_{11}) \nabla (\frac{\delta f}{\delta \phi_n} - \frac{\delta f}{\delta \phi_b})] + g_s.$$

The specific forms of the mixing free energy density function  $f$  will be given in the next section, and the reactive terms will be given below. In the transport equations for the fluid components, an average velocity field  $\mathbf{v}$ , due to non-conservative hydrodynamics, is assumed, whereas the interpenetration or mixing among the components is dictated by the intermolecular (or thermodynamical) interaction potential. From the system of equations for the volume fractions, we can identify the velocity for each individual effective component by accounting for the excessive velocity due to thermodynamical or intermolecular forces. For instance, we identify the solvent velocity as

$$\mathbf{v}_s = \mathbf{v} - \frac{1}{\phi_s} [\alpha_{33} \nabla (\frac{\delta f}{\delta \phi_s} - \frac{1}{2} (\frac{\delta f}{\delta \phi_b} + \frac{\delta f}{\delta \phi_n})) + \frac{1}{2} (\alpha_{22} - \alpha_{11}) \nabla (\frac{\delta f}{\delta \phi_n} - \frac{\delta f}{\delta \phi_b})]. \quad (\text{II.2})$$

Analogously, we can identify the velocity of the EPS and bacteria respectively as

$$\mathbf{v}_n = \mathbf{v} - \frac{1}{\phi_n} [\alpha_{11} \nabla (\frac{\delta f}{\delta \phi_n} - \frac{1}{2} (\frac{\delta f}{\delta \phi_b} + \frac{\delta f}{\delta \phi_s})) + \frac{1}{2} (\alpha_{22} - \alpha_{33}) \nabla (\frac{\delta f}{\delta \phi_s} - \frac{\delta f}{\delta \phi_b})], \quad (\text{II.3})$$

$$\mathbf{v}_b = \mathbf{v} - \frac{1}{\phi_b} [\alpha_{22} \nabla (\frac{\delta f}{\delta \phi_b} - \frac{1}{2} (\frac{\delta f}{\delta \phi_n} + \frac{\delta f}{\delta \phi_s})) + \frac{1}{2} (\alpha_{11} - \alpha_{33}) \nabla (\frac{\delta f}{\delta \phi_s} - \frac{\delta f}{\delta \phi_n})].$$

It then follows that

$$\mathbf{v} = \phi_n \mathbf{v}_n + \phi_b \mathbf{v}_b + \phi_s \mathbf{v}_s. \quad (\text{II.4})$$

So, the bulk velocity is, in fact, a volume averaged velocity.

Acknowledging that the contribution to the velocity of a species vanishes when the species becomes extinct, we approximate the mobility coefficients as

$$\begin{aligned} \alpha_{11} &= \lambda_1 \phi_n (1 - \phi_n), \\ \alpha_{22} &= \lambda_2 \phi_b (1 - \phi_b), \\ \alpha_{33} &= \lambda_3 \phi_s (1 - \phi_s), \end{aligned} \quad (\text{II.5})$$

where  $\lambda_{1,2,3}$  are three constants. In this paper, we only consider the case where the three constants are identical. From (II.5), if we assume  $\lambda_1 = \lambda_2 = \lambda_3 = \lambda$ , we arrive at

$$\begin{aligned}\alpha_{22} - \alpha_{11} &= \lambda\phi_s(\phi_b - \phi_n), \\ \alpha_{22} - \alpha_{33} &= \lambda\phi_n(\phi_b - \phi_s), \\ \alpha_{11} - \alpha_{33} &= \lambda\phi_b(\phi_n - \phi_s).\end{aligned}\tag{II.6}$$

This choice of the coefficients in the mobility matrix yields zero flux for a component when its volume fraction is zero in the mixture.

The velocity for each individual component can then be written as

$$\begin{aligned}\mathbf{v}_s &= \mathbf{v} - \lambda[(1 - \phi_s)\nabla(\frac{\delta f}{\delta\phi_s} - \frac{1}{2}(\frac{\delta f}{\delta\phi_b} + \frac{\delta f}{\delta\phi_n})) + \frac{1}{2}(\phi_b - \phi_n)\nabla(\frac{\delta f}{\delta\phi_n} - \frac{\delta f}{\delta\phi_b})], \\ \mathbf{v}_n &= \mathbf{v} - \lambda[(1 - \phi_n)\nabla(\frac{\delta f}{\delta\phi_n} - \frac{1}{2}(\frac{\delta f}{\delta\phi_b} + \frac{\delta f}{\delta\phi_s})) + \frac{1}{2}(\phi_b - \phi_s)\nabla(\frac{\delta f}{\delta\phi_s} - \frac{\delta f}{\delta\phi_b})], \\ \mathbf{v}_b &= \mathbf{v} - \lambda[(1 - \phi_b)\nabla(\frac{\delta f}{\delta\phi_b} - \frac{1}{2}(\frac{\delta f}{\delta\phi_n} + \frac{\delta f}{\delta\phi_s})) + \frac{1}{2}(\phi_n - \phi_s)\nabla(\frac{\delta f}{\delta\phi_s} - \frac{\delta f}{\delta\phi_n})].\end{aligned}\tag{II.7}$$

The second term on the right hand side of each of the above equations is the excessive velocity for that effective component.

The reactive terms in the transport equations are given by

$$\begin{aligned}g_n &= \mu_0\phi_b\frac{c}{K_c+c}, \\ g_b &= [(\frac{C_1c}{K_1+c} - C_B)\phi_b], \\ g_s &= -(g_n + g_b),\end{aligned}\tag{II.8}$$

and represent conversion among the distinct components through chemical reactions. Here  $\mu_0$  and  $C_1$  measure the maximum growth rate of the EPS and the bacteria, respectively,  $K_c$  and  $K_1$  are the half-saturation constants in the Monod (or Michaelis-Menten) kinetics used in the reaction, and  $C_B$  is a natural decay rate that limits bacteria growth and adds nutrient dependent decay. Note that, if the nutrient value drops low enough,  $c \ll 1$ , then the bacteria will begin to die off. On the other hand, if there is ample nutrient (supposing that excessive nutrient content in the substrate does not inhibit growth), then the  $g_b$  term will act as an exponential growth term of rate  $C_1 - C_B$ . In a realistic scenario, a homeostatic equilibrium can be reached as the bacteria locally exhausts the

nutrient, and the rate of available nutrient (due to diffusion) is counterbalanced by the death term. For simplicity, we will adopt a constant decay rate  $C_B$  in all our numerical studies presented in the paper.

## B. Mixing kinetics

Since the molecular weight of bacteria is normally two orders of magnitudes larger than that of the solvent molecules, we treat it as an effective polymer whose collective behavior is viscous in low concentrations and on the long timescale where growth occurs. As previously mentioned, this treatment is a departure from diffusion-based models which treat biofilm-forming bacteria as passive, or as particles dispersed within the fluid. This approach is most appropriate for relatively dense clusters of bacteria constrained within an extracellular matrix, like those found in growing biofilm colonies. We use the Flory-Huggin's mixing theory [40] to model the mixing phenomena among the EPS, bacteria and the effective solvent.

We denote the mixing free energy density by  $f$ ,

$$f = k_B T \left[ \frac{\gamma_{11}}{2} \|\nabla \phi_n\|^2 + \frac{\gamma_{12}}{2} \|\nabla \phi_b\|^2 + \frac{\gamma_{13}}{2} \|\nabla \phi_s\|^2 + \gamma_2 \left[ \frac{\phi_n}{N_p} \ln \phi_n + \frac{\phi_b}{N_b} \ln \phi_b + \phi_s \ln \phi_s + \chi_{bn} \phi_n \phi_b + \chi_{sb} \phi_s \phi_b + \chi_{sn} \phi_n \phi_s \right] \right], \quad (\text{II.9})$$

where  $k_B$  is the Boltzmann constant,  $T$  is the absolute temperature,  $\gamma_{11,12,13}$  and  $\gamma_2$  measure the strength of the distortional and bulk mixing free energy, respectively, ( $\gamma_{11,12,13}$  have the unit of number per unit length while  $\gamma_2$  is proportional to the number density per unit volume,)  $N_p$  and  $N_b$  denote the polymerization index of the EPS and bacteria, respectively, and  $\chi_{bn, sb, sn}$  are the mixing parameters for the EPS and bacteria, bacteria and solvent, and solvent and EPS, respectively. We remark that we use the simplest possible distortional conformational energy in this mixing free energy density for simplicity. Another choice for the distortional conformational energy can be

$$k_B T \left[ \frac{\gamma_{11}}{2} \|\phi_b \nabla \phi_n - \phi_n \nabla \phi_b\|^2 + \frac{\gamma_{12}}{2} \|\phi_s \nabla \phi_b - \phi_b \nabla \phi_s\|^2 + \frac{\gamma_{13}}{2} \|\phi_n \nabla \phi_s - \phi_s \nabla \phi_n\|^2 \right]. \quad (\text{II.10})$$

In this paper, we stick to the free energy density given in (II.9) and defer the discussion on the other distortional energy to a sequel.

The variation of the free energy density defined by (II.9) with respect to each volume fraction

is given by

$$\begin{aligned}\frac{\delta f}{\delta \phi_n} &= -k_B T \gamma_{11} \Delta \phi_n + \gamma_2 k_B T \left[ \frac{1}{N_p} (\ln(\phi_n) + 1) + \chi_{bn} \phi_b + \chi_{sn} \phi_s \right], \\ \frac{\delta f}{\delta \phi_b} &= -k_B T \gamma_{12} \Delta \phi_b + \gamma_2 k_B T \left[ \frac{1}{N_b} (\ln(\phi_b) + 1) + \chi_{bn} \phi_n + \chi_{sb} \phi_s \right], \\ \frac{\delta f}{\delta \phi_s} &= -k_B T \gamma_{13} \Delta \phi_s + \gamma_2 k_B T \left[ (\ln(\phi_s) + 1) + \chi_{sn} \phi_n + \chi_{sb} \phi_b \right].\end{aligned}\tag{II.11}$$

### C. Constitutive equations

We use the volume fraction of the EPS and bacteria as the primary unknowns. The volume fraction of the solvent is then calculated from the incompressibility constraint

$$\phi_n + \phi_b + \phi_s = 1.\tag{II.12}$$

The mixing free energy in terms of the two unknowns can be recast into

$$\begin{aligned}f &= k_B T \left[ \frac{\gamma_{11}}{2} \|\nabla \phi_n\|^2 + \frac{\gamma_{12}}{2} \|\nabla \phi_b\|^2 + \frac{\gamma_{13}}{2} \|\nabla(\phi_n + \phi_b)\|^2 + \gamma_2 \left[ \frac{\phi_n}{N_p} \ln \phi_n + \frac{\phi_b}{N_b} \ln \phi_b + \right. \right. \\ &\quad \left. \left. (1 - \phi_n - \phi_b) \ln(1 - \phi_n - \phi_b) + \chi_{bn} \phi_n \phi_b + \chi_{sb} (1 - \phi_b - \phi_n) \phi_b + \chi_{sn} \phi_n (1 - \phi_n - \phi_b) \right] \right],\end{aligned}\tag{II.13}$$

The variation of the free energy with respect to the two primary unknowns is given by

$$\delta f = \left( \frac{\delta f}{\delta \phi_n} - \frac{\delta f}{\delta \phi_s} \right) \delta \phi_n + \left( \frac{\delta f}{\delta \phi_b} - \frac{\delta f}{\delta \phi_s} \right) \delta \phi_b.\tag{II.14}$$

Notice that

$$\delta \phi_n = \frac{\partial \phi_n}{\partial t} \delta t = -\nabla \cdot (\mathbf{v} \phi_n) \delta t, \quad \delta \phi_b = \frac{\partial \phi_b}{\partial t} \delta t = -\nabla \cdot (\mathbf{v} \phi_b) \delta t.\tag{II.15}$$

We denote the free energy associated with mixing by

$$\mathcal{A} = \int f d\mathbf{x}.\tag{II.16}$$

Its variation is given by

$$\delta \mathcal{A} = \int \delta f d\mathbf{x} = \int \mathbf{v} \cdot \left[ \phi_n \nabla \left( \frac{\delta f}{\delta \phi_n} - \frac{\delta f}{\delta \phi_s} \right) + \phi_b \nabla \left( \frac{\delta f}{\delta \phi_b} - \frac{\delta f}{\delta \phi_s} \right) \right] \delta t d\mathbf{x}.\tag{II.17}$$

It then follows that

$$\delta f = -\mathbf{v} \cdot \mathbf{F}_e \delta t,\tag{II.18}$$

which implies

$$\begin{aligned} \mathbf{F}_e = & -\phi_n \nabla \left( \frac{\delta f}{\delta \phi_n} - \frac{\delta f}{\delta \phi_s} \right) - \phi_b \nabla \left( \frac{\delta f}{\delta \phi_b} - \frac{\delta f}{\delta \phi_s} \right) = -\gamma_{13} k_B T \nabla \cdot (\nabla \phi_n \nabla \phi_b + \nabla \phi_b \nabla \phi_n) - \\ & \nabla \cdot ((\gamma_{11} + \gamma_{13}) k_B T \nabla \phi_n \nabla \phi_n + (\gamma_{12} + \gamma_{13}) k_B T \nabla \phi_b \nabla \phi_b) + \nabla [\hat{f}(\phi_n, \phi_b) + \\ & \gamma_{11} k_B T (\phi_n \Delta \phi_n + \frac{1}{2} \|\nabla \phi_n\|^2) + \gamma_{12} k_B T (\phi_b \Delta \phi_b + \frac{1}{2} \|\nabla \phi_b\|^2) + \gamma_{13} k_B T (\phi_n \Delta \phi_b + \phi_b \Delta \phi_n + \nabla \phi_n \nabla \phi_b)], \end{aligned} \quad (\text{II.19})$$

where  $\hat{f}$  consists of the bulk terms and their first integrals in the mixing free energy. The first part can be identified as a part of the stress due to inhomogeneity of the volume fractions in the biofilm and the second part serves as an additional pressure in the incompressible material system. So, the elastic stress tensor due to mixing dynamics is given by

$$\tau_{es} = -k_B T [(\gamma_{11} + \gamma_{13}) \nabla \phi_n \nabla \phi_n + (\gamma_{12} + \gamma_{13}) \nabla \phi_b \nabla \phi_b + \gamma_{13} (\nabla \phi_b \nabla \phi_n + \nabla \phi_n \nabla \phi_b)]. \quad (\text{II.20})$$

We proposed two models in [34]. In the first model, we assume the transport and deformation of the active components in the mixture is carried out by the average velocity and its gradient. For instance for the solvent, we assume it is viscous with the stress given by

$$\tau_s = 2\eta_s \mathbf{D}, \quad (\text{II.21})$$

where  $\eta_s$  is the solvent viscosity. If one considers rigid rod-shaped bacteria cells packed close to one another, then at high volume fractions of tightly packed cells, one would expect colloidal effects. However, confocal laser scanning micrographs confirm that the local volume fraction of cells (including the water contained within) is usually less than .2, and below the threshold where these effects occurs [29]. Thus, it is reasonable to assume the bacteria phase is an extended Newtonian fluid and its stress tensor is defined as

$$\tau_b = 2\eta_b(\mathbf{D})\mathbf{D}, \quad (\text{II.22})$$

where  $\eta_b$  is a rate-of-strain dependent viscosity. The EPS polymer network is assumed viscoelastic with stress  $a\phi_n \tau_n$ , where  $\tau_n$  obeys the Johnson-Segalman equation

$$\frac{d}{dt} \tau_n - \mathbf{W} \cdot \tau_n + \tau_n \cdot \mathbf{W} - a[\mathbf{D} \cdot \tau_n + \tau_n \cdot \mathbf{D}] + \frac{1}{\lambda_1} \tau_n = 2 \frac{\eta_p}{\lambda_1} \mathbf{D}, \quad (\text{II.23})$$

where  $\frac{d}{dt} = \frac{\partial}{\partial t} + \mathbf{v} \cdot \nabla$  is the material derivative,  $\mathbf{W}$  is the vorticity tensor,  $a$  is a rate parameter in  $[-1, 1]$ ,  $\eta_p$  is the polymeric viscosity and  $\lambda_1$  is the relaxation time. Since the velocity gradient used in this constitutive model is calculated from the average velocity, we name it the VA model.

If we assume the transport of each component is carried out by their respective velocity fields and the associated gradients, alternative constitutive equations for the stress tensors are proposed as follows

$$\tau_s = 2\eta_s \mathbf{D}_s, \quad \tau_b = 2\eta_b \mathbf{D}_b, \quad (II.24)$$

$$\frac{d}{dt} \tau_n - \mathbf{W}_n \cdot \tau_n + \tau_n \cdot \mathbf{W}_n - a[\mathbf{D}_n \cdot \tau_n + \tau_n \cdot \mathbf{D}_n] + \frac{1}{\lambda_1} \tau_n = 2 \frac{\eta_2}{\lambda_1} \mathbf{D}_n,$$

where  $\mathbf{D}_s, \mathbf{D}_b, \mathbf{D}_n$  are the rate of strain tensors calculated using the respective velocity field  $\mathbf{v}_s, \mathbf{v}_b, \mathbf{v}_n$ ,  $\mathbf{W}_n$  is the vorticity tensor calculated from  $\mathbf{v}_n$  and  $\frac{d}{dt} = \frac{\partial}{\partial t} + \mathbf{v}_n \cdot \nabla$  is the material derivative for the EPS strand transported via the polymer network velocity. We refer to this constitutive model the VN model.

#### D. Transport of the nutrient

The transport of nutrient is carried out by the solvent velocity  $\mathbf{v}_s$ :

$$\frac{\partial}{\partial t} (\phi_s c) + \nabla \cdot (c \mathbf{v}_s \phi_s - D_s \phi_s \nabla c) = g_c, \quad (II.25)$$

where  $D_s$  is the diffusion coefficient for the nutrient. The nutrient decay rate is proportional to the bacterial consumption,

$$g_c = -C_2 \phi_b \frac{c}{K_2 + c}, \quad (II.26)$$

where  $C_2$  parametrizes the uptake rate of the nutrient, and  $K_2$  is the half saturation constant for nutrient consumption. We neglect the possible conversion between EPS and nutrient in this model.

#### E. Summary of the governing system of equations

The governing system of equations for the biofilm-solvent mixture are summarized below.

*Transport equations for the volume fractions:*

$$\begin{aligned}
\frac{\partial \phi_n}{\partial t} + \nabla \cdot (\phi_n \mathbf{v}) &= \nabla \cdot [\lambda \phi_n (1 - \phi_n) \nabla (\frac{\delta f}{\delta \phi_n} - \frac{1}{2} (\frac{\delta f}{\delta \phi_b} + \frac{\delta f}{\delta \phi_s})) + \frac{\lambda}{2} \phi_n (\phi_b - \phi_s) \nabla (\frac{\delta f}{\delta \phi_s} - \frac{\delta f}{\delta \phi_b})] + g_n, \\
\frac{\partial \phi_b}{\partial t} + \nabla \cdot (\phi_b \mathbf{v}) &= \nabla \cdot [\lambda \phi_b (1 - \phi_b) \nabla (\frac{\delta f}{\delta \phi_b} - \frac{1}{2} (\frac{\delta f}{\delta \phi_n} + \frac{\delta f}{\delta \phi_s})) + \frac{\lambda}{2} \phi_b (\phi_n - \phi_s) \nabla (\frac{\delta f}{\delta \phi_s} - \frac{\delta f}{\delta \phi_n})] + g_b, \\
\frac{\partial \phi_s}{\partial t} + \nabla \cdot (\phi_s \mathbf{v}) &= \nabla \cdot [\lambda \phi_s (1 - \phi_s) \nabla (\frac{\delta f}{\delta \phi_s} - \frac{1}{2} (\frac{\delta f}{\delta \phi_b} + \frac{\delta f}{\delta \phi_n})) + \frac{\lambda}{2} \phi_s (\phi_b - \phi_n) \nabla (\frac{\delta f}{\delta \phi_n} - \frac{\delta f}{\delta \phi_b})] + g_s,
\end{aligned} \tag{II.27}$$

$$g_n = \mu_0 \phi_b \frac{c}{K_c + c},$$

$$g_b = [(\frac{C_1 c}{(K_1 + c)} - C_B)] \phi_b,$$

$$g_s = -(g_n + g_b).$$

*Individual velocity for each effective component:*

$$\begin{aligned}
\mathbf{v}_s &= \mathbf{v} - \lambda [(1 - \phi_s) \nabla (\frac{\delta f}{\delta \phi_s} - \frac{1}{2} (\frac{\delta f}{\delta \phi_b} + \frac{\delta f}{\delta \phi_n})) + \frac{1}{2} (\phi_b - \phi_n) \nabla (\frac{\delta f}{\delta \phi_n} - \frac{\delta f}{\delta \phi_b})], \\
\mathbf{v}_n &= \mathbf{v} - \lambda [(1 - \phi_n) \nabla (\frac{\delta f}{\delta \phi_n} - \frac{1}{2} (\frac{\delta f}{\delta \phi_b} + \frac{\delta f}{\delta \phi_s})) + \frac{1}{2} (\phi_b - \phi_s) \nabla (\frac{\delta f}{\delta \phi_s} - \frac{\delta f}{\delta \phi_b})], \\
\mathbf{v}_b &= \mathbf{v} - \lambda [(1 - \phi_b) \nabla (\frac{\delta f}{\delta \phi_b} - \frac{1}{2} (\frac{\delta f}{\delta \phi_n} + \frac{\delta f}{\delta \phi_s})) + \frac{1}{2} (\phi_n - \phi_s) \nabla (\frac{\delta f}{\delta \phi_s} - \frac{\delta f}{\delta \phi_n})].
\end{aligned} \tag{II.28}$$

*Transport equation for the nutrient:*

$$\frac{\partial (c \phi_s)}{\partial t} + \nabla \cdot (\mathbf{v}_s c \phi_s) = \nabla \cdot \phi_s D_s \nabla c - (C_2 \phi_b \frac{c}{K_2 + c}). \tag{II.29}$$

*Continuity equation and the momentum balance equation:*

$$\nabla \cdot \mathbf{v} = 0,$$

$$\begin{aligned}
\rho \frac{d\mathbf{v}}{dt} &= \nabla \cdot (a \phi_n \boldsymbol{\tau}_n + \phi_b \boldsymbol{\tau}_b + \phi_s \boldsymbol{\tau}_s) - \nabla \cdot [p \mathbf{I} + k_B T ((\gamma_{11} + \gamma_{13}) \nabla \phi_n \nabla \phi_n + (\gamma_{12} + \gamma_{13}) \nabla \phi_b \nabla \phi_b \\
&\quad + \gamma_{13} (\nabla \phi_n \nabla \phi_b + \nabla \phi_b \nabla \phi_n))].
\end{aligned} \tag{II.30}$$

Here,  $\rho = \phi_s \rho_s + \phi_b \rho_b + \phi_n \rho_n$  is the density of the mixture. The stress constitutive equations are given by eq. (II.21),(II.22),(II.23) or (II.24).

**Remarks:**

- We note that the elastic stress constitutive equation is valid only within the domain where  $\phi_n \neq 0$ . Hence, its contribution is zero in the pure solvent region. For computational convenience, a transport equation for the stress component  $\sigma_n = \phi_n \tau_n$  can be formulated to have a globally valid constitutive equation for the elastic stress.
- The continuity equation is upheld approximately under the assumption that the mobility  $\lambda$  is small and the density differences among the three effective components are not far apart.

### III. NONDIMENSIONALIZATION

We use a characteristic time scale  $t_0$ , a characteristic length scale  $h$ , and a characteristic nutrient concentration  $c_0$  to nondimensionalize the variables

$$\tilde{t} = \frac{t}{t_0}, \tilde{\mathbf{x}} = \frac{\mathbf{x}}{h}, \tilde{\mathbf{v}} = \frac{\mathbf{v}t_0}{h}, \tilde{p} = \frac{ph^2}{f_0}, \tilde{\boldsymbol{\tau}} = \frac{\boldsymbol{\tau}h^2}{f_0}, \tilde{c} = \frac{c}{c_0}, \quad (\text{III.1})$$

where  $f_0$  is a characteristic force scale. The following dimensionless parameters arise

$$\Lambda = \frac{\lambda t_0 f_0}{h^4}, \Gamma_{1j} = \frac{\gamma_{1j} k_B T}{f_0}, j = 1, 2, 3, \Gamma_2 = \frac{\gamma_2 k_B T h^2}{f_0}, Re_s = \frac{f_0 t_0}{\eta_s h^2}, Re_b = \frac{f_0 t_0}{\eta_b h^2}, Re_p = \frac{f_0 t_0}{\eta_p h^2}, \tilde{D}_s = \frac{D_s t_0}{h^2},$$

$$Bi = \frac{\rho_0 h^4}{f_0 t_0^2}, \tilde{\rho} = Bi (\phi_s \frac{\rho_s}{\rho_0} + \phi_n \frac{\rho_n}{\rho_0} + \phi_b \frac{\rho_b}{\rho_0}), \tilde{\mu}_0 = \mu_0 t_0, \tilde{K}_c = \frac{K_c}{c_0}, \tilde{K}_i = \frac{K_i}{c_0}, i = 1, \dots, 2, \quad (\text{III.2})$$

$$\Lambda_1 = \frac{\lambda_1}{t_0}, \tilde{C}_1 = C_1 t_0, C_2 = C_2 t_0, \tilde{C}_B = C_B t_0.$$

where  $\tilde{\rho}_0$  is an average density,  $Re_s$ ,  $Re_b$  and  $Re_p$  are the Reynolds number for the solvent, the bacteria and the EPS, respectively, and  $\Lambda_1$  is the Deborah number for the EPS. We set  $Bi = 1$  and, thus, the force scale is chosen as  $f_0 = \frac{\rho_0 h^4}{t_0^2}$ .

For simplicity, we drop the  $\tilde{\phantom{x}}$  on the dimensionless variables and the parameters. The system of

governing equations in these dimensionless variables is given by

$$\frac{\partial \phi_n}{\partial t} + \nabla \cdot (\phi_n \mathbf{v}) = \nabla \cdot [\Lambda \phi_n ((1 - \phi_n) \nabla (\frac{\delta f}{\delta \phi_n} - \frac{1}{2} (\frac{\delta f}{\delta \phi_b} + \frac{\delta f}{\delta \phi_s})) + \frac{1}{2} (\phi_b - \phi_s) \nabla (\frac{\delta f}{\delta \phi_s} - \frac{\delta f}{\delta \phi_b}))] + g_n,$$

$$\frac{\partial \phi_b}{\partial t} + \nabla \cdot (\phi_b \mathbf{v}) = \nabla \cdot [\Lambda \phi_b ((1 - \phi_b) \nabla (\frac{\delta f}{\delta \phi_b} - \frac{1}{2} (\frac{\delta f}{\delta \phi_n} + \frac{\delta f}{\delta \phi_s})) + \frac{1}{2} (\phi_n - \phi_s) \nabla (\frac{\delta f}{\delta \phi_s} - \frac{\delta f}{\delta \phi_n}))] + g_b,$$

$$g_n = \mu_0 \phi_b \frac{c}{K_c + c},$$

$$g_b = [(\frac{C_1 c}{(K_1 + c)} - C_B)] \phi_b,$$

$$\frac{\partial (c \phi_s)}{\partial t} + \nabla \cdot (\mathbf{v}_s c \phi_s) = \nabla \cdot D_s \phi_s \nabla c - (C_2 \phi_b \frac{c}{K_2 + c}), \quad (\text{III.3})$$

$$\nabla \cdot \mathbf{v} = 0,$$

$$\rho \frac{d\mathbf{v}}{dt} = \nabla \cdot (a \phi_n \boldsymbol{\tau}_n + \phi_b \boldsymbol{\tau}_b + \phi_s \boldsymbol{\tau}_s) - \nabla \cdot [p \mathbf{I} + k_B T ((\Gamma_{11} + \Gamma_{13}) \nabla \phi_n \nabla \phi_n + (\Gamma_{12} + \Gamma_{13}) \nabla \phi_b \nabla \phi_b +$$

$$\Gamma_{13} (\nabla \phi_n \nabla \phi_b + \nabla \phi_b \nabla \phi_n))],$$

where  $\rho = \phi_s \rho_s + \phi_b \rho_b + \phi_n \rho_n$ . The constitutive equations for the VA model are given by

$$\Lambda_1 \left[ \frac{\partial}{\partial t} \boldsymbol{\tau} + \mathbf{v} \cdot \nabla (\boldsymbol{\tau}) - \mathbf{W} \cdot \boldsymbol{\tau} + \boldsymbol{\tau} \cdot \mathbf{W} - a [\mathbf{D} \cdot \boldsymbol{\tau} + \boldsymbol{\tau} \cdot \mathbf{D}] \right] + \boldsymbol{\tau} = \frac{2}{Re_p} \mathbf{D}, \quad (\text{III.4})$$

$$\boldsymbol{\tau}_b = \frac{2}{Re_b} \mathbf{D}, \boldsymbol{\tau}_s = \frac{2}{Re_s} \mathbf{D}.$$

The mixing free energy density is now given by

$$f = \frac{\Gamma_{11}}{2} \|\nabla \phi_n\|^2 + \frac{\Gamma_{12}}{2} \|\nabla \phi_b\|^2 + \frac{\Gamma_{13}}{2} \|\nabla \phi_s\|^2 + \Gamma_2 \left[ \frac{\phi_n}{N_p} \ln \phi_n + \frac{\phi_b}{N_b} \ln \phi_b + \phi_s \ln \phi_s + \right. \quad (\text{III.5})$$

$$\left. \chi_{bn} \phi_n \phi_b + \chi_{sb} \phi_s \phi_b + \chi_{sn} \phi_n \phi_s \right].$$

The no-flux boundary conditions at the solid impermeable boundary are derived from the transport equations for the volume fractions

$$\mathbf{n} \cdot [\phi_n ((1 - \phi_n) \nabla (\frac{\delta f}{\delta \phi_n} - \frac{1}{2} (\frac{\delta f}{\delta \phi_b} + \frac{\delta f}{\delta \phi_s})) + \frac{1}{2} (\phi_b - \phi_s) \nabla (\frac{\delta f}{\delta \phi_s} - \frac{\delta f}{\delta \phi_b}))] = 0, \quad (\text{III.6})$$

$$\mathbf{n} \cdot [\phi_b ((1 - \phi_b) \nabla (\frac{\delta f}{\delta \phi_b} - \frac{1}{2} (\frac{\delta f}{\delta \phi_n} + \frac{\delta f}{\delta \phi_s})) + \frac{1}{2} (\phi_n - \phi_s) \nabla (\frac{\delta f}{\delta \phi_s} - \frac{\delta f}{\delta \phi_n}))] = 0,$$

where  $\mathbf{n}$  is the unit external normal of the boundary. In addition, we impose the following boundary conditions at the solid boundary:

$$\mathbf{v} = \mathbf{0}, \mathbf{n} \cdot \nabla \phi_n = 0, \mathbf{n} \cdot \nabla \phi_b = 0. \quad (\text{III.7})$$

Along the same boundary, we impose a no-flux condition for the nutrient as well:

$$\mathbf{n} \cdot \nabla c = 0. \quad (\text{III.8})$$

Analogously, if the nutrient is fed along a certain part of the boundary, we impose

$$c = c_b \quad (\text{III.9})$$

along that part of the boundary. For the simulations in Section 4, we impose a periodic boundary condition in one space-direction and the above boundary conditions in the transverse direction.

We denote the bulk free energy density as

$$\hat{f} = \Gamma_2 \left[ \frac{\phi_n}{N_p} \ln \phi_n + \frac{\phi_b}{N_b} \ln \phi_b + \phi_s \ln \phi_s + \chi_{bn} \phi_n \phi_b + \chi_{sb} \phi_s \phi_b + \chi_{sn} \phi_n \phi_s \right]. \quad (\text{III.10})$$

In practice, we regularize the bulk free energy by the following in case of  $\phi_n = 0$  and/or  $\phi_b = 0$ :

$$\begin{aligned} \hat{f} = \Gamma_2 \left[ \frac{\phi_n}{N_p} \ln(\phi_n + \Delta\phi_n^0) + \frac{\phi_b}{N_b} \ln(\phi_b + \Delta\phi_b^0) + \phi_s \ln \phi_s + \right. \\ \left. \chi_{bn} \phi_n \phi_b + \chi_{sb} \phi_s \phi_b + \chi_{sn} \phi_n \phi_s \right], \end{aligned} \quad (\text{III.11})$$

where  $\Delta\phi_n^0$  and  $\Delta\phi_b^0$  are two small positive quantities. Note that we don't need to regularize  $\phi_s$  because, as mentioned previously, the bulk of the biofilm is composed primarily of water and, thus,  $\phi_s > 0$  in the biofilm mixture all the time

It is worth noting here that our choice of characteristic timescale  $t_0$  depends upon the physical phenomenon that we are interested in modeling, and has serious repercussions on the numerical stability of the scheme used to solve the equation. In fact, we could identify fast, slow, and intermediate timescales in the problem and propose some simplifications in the case of very fast or very slow timescales. In the slow time scale on which biofilm growth can be observed, the elastic response of the system is minimal and, thus, system can be treated collectively as viscous. In the fast and intermediate time scales, the elastic response of the EPS network needs to be accounted for by a viscoelastic constitutive model (II.24). In the following numerical simulations, we will focus on biofilm-flow interaction in the slow time scale:  $\Lambda_1 \ll 1$ . The elastic stress in the VA model (II.23) is given by  $\boldsymbol{\tau}_n \approx 2\eta_n \mathbf{D}$ .

#### IV. NUMERICAL SIMULATION OF TRANSIENT 2-D BIOFILM DYNAMICS

We present numerical solutions for transient states of the ternary biofilm model using the VA model. In this section, we will investigate the growth of a biofilm in 2-D:  $(x, y) \in I = [0, L] \times [0, 1]$ , governed by the equations given in the previous section. We consider a 2-D initial-boundary value problem with prescribed initial states:

$$\phi_n(x, y, 0) = \phi_n^0(x, y), \phi_b(x, y, 0) = \phi_b^0(x, y), c(x, y, 0) = c^0(x, y), d(x, y, 0) = d^0(x, y), \quad (\text{IV.1})$$

and boundary conditions given by (III.6-III.9). All physical variables are assumed periodic in the x-direction. In the y-direction, we assume a flux-free boundary condition for the volume fractions at both walls and the same type of boundary condition for the nutrient concentration at one side  $y = 0$ ; we feed in the nutrient at the upper boundary,

$$c|_{y=1}(x) = c^*, \quad (\text{IV.2})$$

which allows the possibility of variable nutrient feeding in time. We assume the velocity at  $y = 0$  is  $\mathbf{v} = \mathbf{0}$  and  $\mathbf{v}(y = 1) = (v_0, 0)$ , where  $v_0$  is a shear speed.

##### A. Numerical Schemes

We use the finite difference method to solve the coupled flow, phase field, and nutrient concentration transport equation. We employ uniform spatial and time step sizes denoted by  $\Delta x, \Delta y$  and  $\Delta t$  respectively. The superscript  $n$  denotes the discretized solution at time level  $n\Delta t$ . We solve the coupled momentum transport equation and the continuity equation using a Gauge-Uzawa scheme, developed by Shen et al. [41], and the other transport equations using semi-implicit finite difference schemes.

We denote

$$\begin{aligned} \mathbf{R} = & -\nabla \cdot ((\Gamma_{11} + \Gamma_{13})\nabla\phi_n\nabla\phi_n + (\Gamma_{12} + \Gamma_{13})\nabla\phi_b\nabla\phi_b + \Gamma_{13}(\nabla\phi_n\nabla\phi_b + \nabla\phi_b\nabla\phi_n)) + \\ & \nabla \cdot (a\phi_n\boldsymbol{\tau}_n + \phi_b\boldsymbol{\tau}_b + \phi_s\boldsymbol{\tau}_s - \frac{2}{Re_a}\mathbf{D}), \end{aligned} \quad (\text{IV.3})$$

where  $Re_a$  is an averaged Reynolds number. Preferably, it is chosen such that

$$\frac{1}{Re_a} = \frac{1}{|\Omega|} \int_{\Omega} \left( \frac{a\phi_n}{Re_n} + \frac{\phi_b}{Re_b} + \frac{\phi_s}{Re_s} \right) d\mathbf{x}, \quad (\text{IV.4})$$

where  $\Omega$  is the computational domain. The momentum transport equation can be rewritten as

$$\rho \left( \frac{\partial}{\partial t} \mathbf{v} + \mathbf{v} \cdot \nabla \mathbf{v} \right) = -\nabla p + \frac{1}{Re_a} \nabla^2 \mathbf{v} + \mathbf{R}. \quad (\text{IV.5})$$

The nonlinear term  $\mathbf{R}$  is treated explicitly through extrapolation. We calculate  $\mathbf{v}$  and the pressure in three steps. We present the scheme for the case of periodic boundary conditions in the  $x$  direction and physical boundary conditions in the  $y$  direction. For simplicity, the second order extrapolation of any function  $f$  is denoted by  $\bar{f}^{n+1} = 2f^n - f^{n-1}$ .

Step 1:

$$\begin{cases} \rho^{n+1} \left[ \frac{\mathbf{u}^{n+1} - \mathbf{v}^n}{\Delta t} \right] + \rho^{n+1} \bar{\mathbf{v}}^{n+1} \cdot \nabla \mathbf{u}^{n+1} + \frac{1}{Re_a} [\nabla s^n - \nabla^2 \mathbf{u}^{n+1}] = \bar{\mathbf{R}}^{n+1}, \\ \mathbf{u}^{n+1}|_{y=0} = 0, \mathbf{u}^{n+1}|_{y=1} = \mathbf{v}_0. \end{cases} \quad (\text{IV.6})$$

Step 2: We implement the projection step by solving a Poisson equation with the Neumann boundary condition:

$$\begin{cases} -\nabla \cdot \left( \frac{1}{\rho^{n+1}} \nabla \psi^{n+1} \right) = \nabla \cdot \mathbf{u}^{n+1}, \\ \frac{\partial \psi^{n+1}}{\partial n} \Big|_{y=0,1} = 0. \end{cases} \quad (\text{IV.7})$$

Step 3: We correct the velocity, pressure and the auxiliary variable  $s$ .

$$\begin{cases} \mathbf{v}^{n+1} = \mathbf{u}^{n+1} + \frac{1}{\rho^{n+1}} \nabla \psi^{n+1}, \\ s^{n+1} = s^n - \nabla \cdot \mathbf{u}^{n+1}, \\ p^{n+1} = -\frac{\psi^{n+1}}{\Delta t} + \frac{1}{Re_a} s^{n+1}, \end{cases} \quad (\text{IV.8})$$

where  $s^0 = 0$ . This is a first order scheme in time.

The polymer volume fraction at time step  $n + 1$  governed by the Cahn-Hilliard equation is calculated by:

$$\frac{\phi_n^{n+1} - \phi_n^n}{\Delta t} + \theta \Lambda \nabla \cdot \Phi_n^{n+1} = \bar{g}_n^{n+\theta} - (1 - \theta) \Lambda \nabla \cdot \Phi_n^n - \overline{NL}_n^{n+\theta}, \quad (\text{IV.9})$$

where the semi-implicit and explicit terms are split (the nonlinear terms, including the natural log terms from the free energy and from the growth rate, are extrapolated). For readability, we have

introduced symbols corresponding to the explicit and semi-implicit/extrapolated pieces:

$$\begin{aligned}
\Phi_n^{n+1} &= \bar{\phi}_n^{n+\theta}(1 - \bar{\phi}_n^{n+\theta})\nabla_y [(-\Gamma_{11} - .5\Gamma_{13})\Delta\phi_n^{n+1} - .5(-\Gamma_{12} + \Gamma_{13})\Delta\phi_b^{n+1} + \\
&+ \Gamma_2(-1.5\chi_{sn} - .5\chi_{bn} + .5\chi_{sb})\phi_n^{n+1} + \Gamma_2(\chi_{bn} - \chi_{sn})\phi_b^{n+1}] + \\
&+ \bar{\phi}_n^{n+\theta}(2\bar{\phi}_b^{n+\theta} + \bar{\phi}_n^{n+\theta} - 1)\nabla_y [.5\Gamma_{13}\Delta\phi_n^{n+1} + .5(\Gamma_{12} + \Gamma_{13})\Delta\phi_b^{n+1} \\
&+ .5\Gamma_2(\chi_{sn} - \chi_{bn} + \chi_{sb})\phi_n^{n+1} + \Gamma_2\chi_{sb}\phi_b^{n+1}], \tag{IV.10}
\end{aligned}$$

$$\begin{aligned}
\overline{NL}^{n+1} &= \bar{\phi}_n^{n+\theta}(1 - \bar{\phi}_n^{n+\theta})\nabla_y \left( \frac{1}{N_p}(\ln(\bar{\phi}_n^{n+\theta} + \Delta\phi_n^0) + 1) - \frac{1}{2N_b}(\ln(\bar{\phi}_b^{n+\theta} + \Delta\phi_b^0) + 1) + \ln\bar{\phi}_s^{n+\theta} \right) \\
&+ \bar{\phi}_n^{n+\theta}(2\bar{\phi}_b^{n+\theta} + \bar{\phi}_n^{n+\theta} - 1)\nabla_y \left( -\frac{1}{N_b}(\ln(\bar{\phi}_b^{n+\theta} + \Delta\phi_b^0) + 1) + \ln\bar{\phi}_s^{n+\theta} \right).
\end{aligned}$$

A similar update scheme is employed for the other phase variable  $\phi_b$ . Here the  $\theta$ -method is employed for  $0 \leq \theta \leq 1$  and  $\theta = 1/2$  gives the semi-implicit, second order in time Crank-Nicholson algorithm. Here, all of the “bar” terms are extrapolated values at the intermediate timestep:

$(\bar{\cdot})^{n+\theta} = (1 - \theta)(\cdot)^n + \theta(\cdot)^{n+1}$ . The update scheme for the nutrient transport equation is:

$$\frac{1}{\Delta t}(\phi_s^{n+1}c^{n+1} - \phi_s^{n+1}c^n) - \theta\nabla \cdot (D_s\phi_s^{n+1}\nabla c^{n+1}) = (1 - \theta)\nabla \cdot (D_s\phi_s^n\nabla c^n) - \bar{g}_c^{n+\theta} - \nabla \cdot (\bar{c}^{n+\theta}\bar{\mathbf{v}}_s^{n+\theta}\bar{\phi}_s^{n+\theta}), \tag{IV.11}$$

where the  $\phi_s^{n+1}$  is computed by updating the phase field equations, using the above scheme, prior to updating the concentration of nutrient substrates. The spatial discretization in the above semidiscretized equations is done using central differences to ensure at least second order accuracy in space as well as to respect symmetry.

The boundary conditions at the top and bottom boundary  $y = 1, 0$  are handled in the following way. We use uniform mesh size in both the spatial and temporal discretization, where the time step size is  $\Delta t$  and spatial mesh size is  $\Delta x = L/M_x, \Delta y = 1/M_y$ . The computation domain  $\Omega = [0, L] \times [0, 1]$  is divided into uniform cells by nodes  $(x_i, y_j) = (i\Delta x, j\Delta y)$ ,  $i = 0, \dots, M_x, j = 0, \dots, M_y$ . We denote the value of the numerical solution of (IV.10) and (IV.11) at  $(n\Delta t, i\Delta x, j\Delta y)$  by  $\phi_{n,i,j}^n, c_{i,j}^n$  respectively. For either the case of the cavity geometry or the shear flow, we have  $\mathbf{v} \cdot \mathbf{n}|_{0,1} = 0$ . Thus the boundary conditions for  $\phi_n, \phi_b$ , and  $c$  given by (III.6)-(III.9) yield the discrete forms of the boundary conditions

$$\phi_{n,b,i,1}^n = \phi_{n,b,i,-1}^n, \phi_{n,b,i,2}^n = \phi_{n,b,i,-2}^n, \phi_{n,b,i,M_y+1}^n = \phi_{n,b,i,M_y-1}^n, \phi_{n,b,i,M_y+2}^n = \phi_{n,b,i,M_y-2}^n, \tag{IV.12}$$

$$c_{i,1}^n = c_{i,-1}^n, c_{i,M_y+1}^n = c_{i,M_y-1}^n, \quad i = 0, \dots, M_x.$$

The numerical scheme for the volume fractions and nutrient concentration is second order in space and second order in time if we choose  $\theta = 1/2$ . The overall scheme however is first order

in time and second order in space. To ensure accuracy in time, second order extrapolation is used for the  $\mathbf{R}$  term in the momentum transport equation (IV.6) and the nonlinear terms in the phase field equations (IV.9). The density of the solvent, bacteria and polymer network are set to be the same in this study, thus  $\rho^n$  is in fact a constant. The average Reynolds number  $Re_a$  is computed by  $\frac{1}{Re_a} = \frac{\phi_n^{max}}{Re_n} + \frac{\phi_b^{max}}{Re_b} + \frac{(1-\phi_n^{max}-\phi_b^{max})}{Re_s}$ , where  $\phi_n^{max} = \max\{\phi_{n,i,j}, 0 \leq i \leq M_x, 0 \leq j \leq M_y\}$  and  $\phi_b^{max}$  is evaluated at the same location. Thus  $Re_a$  and is a constant at each time step  $t_n$ , but varies with time. For convenience, we set  $L = 1$ . All numerical results presented below are for at least  $\Delta x = \Delta y = \frac{1}{128}$ .

The entire numerical scheme is executed in each time step in the following order.

- First, the velocity and the pressure field are solved.
- Second, the volume fractions are updated.
- Finally, the nutrient concentration is computed.

The numerical scheme is implemented in both regular and staggered grids in 2 space dimension. Convergence rates in both space and time are verified through extensive mesh refinement numerical experiments. These techniques are appropriate for  $Re \leq O(10)$ , which is in the laminar flow regime.

## B. Numerical Results and Discussions

Before taking a look at several numerical simulations of biofilm flow interaction, it is necessary to examine the way the various parameters affect the evolution of biofilm mixing and biofilm growth in "quiescent fluids". The polymer parameters (top third of Table 1), are picked in the regime of a gel-like biofilm where channel formation is known to occur [42]. The Flory-Huggins constants (besides  $\chi_{bn}$ ) are picked to promote the formation of a stable gel fraction [37], though the dynamics due to intermixing of the components is more complicated in this ternary model. The mixing parameter  $\chi_{bn}$  is set to zero to accommodate the fact the EPS is tied to the cell from which it grows. The other Flory-Huggins parameters are based upon previous biofilm modeling attempts [24, 25].

Growth related constants are given in the middle third of Table 2. Due to the abundance of literature studying the effects of oxygen content on bacteria and biofilm growth, we will treat

Symbol	Parameter	Value	Unit
T	Temperature	303	Kelvin
$\gamma_1$	Distortional energy	$8 \times 10^6$	$\text{m kg s}^{-2}$
$\gamma_2$	Strength of the bulk mixing energy	$3 \times 10^{17}$	$\text{m kg s}^{-2}$
$\chi_{sn}$	Flory-Huggins mixing parameter	.25	dimensionless
$\chi_{sb}$	Flory-Huggins mixing parameter	.25	dimensionless
$\chi_{bn}$	Flory-Huggins mixing parameter	0	dimensionless
$\lambda$	Mobility parameter	$1 \times 10^{-10}$	$\text{kg}^{-1} \text{m}^3 \text{s}$
$\lambda_1$	polymer relaxation time	100	s
$N_b$	Generalized polymerization parameter (Bacteria)	1000	dimensionless
$N_n$	Generalized polymerization parameter (EPS)	1000	dimensionless
$\mu_0$	Maximum EPS production rate	$1.5 \times 10^{-4}$	$\text{s}^{-1}$
$K_c$	Half saturation constant for polymer growth	$3.5 \times 10^{-4}$	$\text{kg m}^{-3}$
$C_1$	Maximum bacterial mode growth rate	$1.5 \times 10^{-4}$	$\text{s}^{-1}$
$K_1$	Half saturation constant for bacterial mode growth	$3.5 \times 10^{-4}$	$\text{kg m}^{-3}$
$C_B$	Average bacteria death rate	$2 \times 10^{-7}$ or $2 \times 10^{-5}$	$\text{s}^{-1}$
$D_s$	Substrate diffusion constant	$2 \times 10^{-9}$	$\text{m}^2 \text{s}^{-1}$
$C_2$	Maximum nutrient consumption rate	$2 \times 10^{-3}$	$\text{kg m}^{-3} \text{s}^{-1}$
$K_2$	Nutrient uptake constant	$3.5 \times 10^{-4}$	$\text{kg m}^{-3}$
$\eta_p$	Viscosity of the EPS network	$4.3 \times 10^2$	$\text{kg m}^{-1} \text{s}^{-1}$
$\eta_s$	Viscosity of the solvent	$1.002 \times 10^{-3}$	$\text{kg m}^{-1} \text{s}^{-1}$
$\eta_b$	Viscosity of the bacteria in solvent	$4.3 \times 10^{-1}$	$\text{kg m}^{-1} \text{s}^{-1}$
$\rho_n$	Network density	$1 \times 10^3$	$\text{kg m}^{-3}$
$\rho_s$	Solvent density	$1 \times 10^3$	$\text{kg m}^{-3}$
$\rho_b$	Bacteria density	$1 \times 10^3$	$\text{kg m}^{-3}$
$h$	Characteristic length scale	$1 \times 10^{-3}$	m
$t_0$	Characteristic time scale	$1 \times 10^3$ (growth)	s
$c_0$	Characteristic concentration	$1 \times 10^{-3}$	$\text{kg m}^{-3}$
$\rho_0$	Characteristic density ( $=\rho_s$ )	$1 \times 10^3$	$\text{kg m}^{-3}$

TABLE I. Parameter values used in simulations (unless otherwise specified). Only values relevant to the simulations are given here.

our nutrient concentration  $c$  as the local oxygen concentration. The maximal growth rates and associated half-saturation and diffusion constants are the same used in other modeling efforts based upon experimental results [16, 22, 37, 43] for growth rates of biofilms relative to oxygen concentration.

The bottom third of Table 3 contains typical fluid parameters [44]. On the timescale of days, where visible growth occurs, the fluid can be treated as viscous [36, 37]. Thus, we neglect the elastic contribution of the bulk stress for the simulations below. The viscosities and other fluid parameters are consistent with other modeling efforts [1, 24, 25, 37] and should allow for easy comparison with those models.

### *1. Growth in quiescent fluids*

We begin our discussion of the numerical simulations by focusing on the basic mechanics of biofilm growth. We simulate biofilm growth in a quiescent water bed, where the nutrient (oxygen) is fed at the upper boundary (interface with the ambient air) ( $y = 1$ ) while periodic boundary conditions are assumed in the  $x$  direction. Unless otherwise specified, we assume the nutrient concentration at the upper interface is fixed  $c(x, 1) = 1$  throughout the simulation. Figures 1-3 show some representative numerical results of this simulation at selected time values. Figure 1 depicts the distribution of the EPS volume fraction and the bacterial volume fraction at three time values during the course of simulated growth, representing the initial, the intermediate and the mature stage.

The initial condition for this growth simulation is that the bacteria are populated lightly in the bottom of a water tank with a very low EPS concentration. As the by-product of the bacterial growth, EPS grows as the bacteria multiply. The stratification in both the EPS and bacteria is captured well by the simulation. Although the average (macroscopic) velocity of the system is near zero, which justifies the use of quiescent fluids, there exists the excessive velocity for each component to “move” due to inter-component mixing. Here, the biofilm growth profile respects the normal mode analysis, obtained on constant equilibria, which predicts that the growth rates differentiate based on the scale of the underlying perturbation of volume fractions, i.e., the fastest growth is dedicated to a certain range of wave numbers and the growth (expansion) phenomenon is associated with long and intermediate wave disturbances only [34].

As the initial bacterial distribution is nearly uniform, it quickly becomes heterogeneous during

growth. The bacteria tend to aggregate or nucleate behind the fastest growing hump leaving behind a less populated landscape. This phenomenon seems to be duplicated in the EPS production, which is expected given that the EPS is produced by the cells. In the near mature stage of growth, the high concentration of the bacteria and EPS are observed in the nucleated hump. This nucleated growth profile has been observed in other models [21, 25], and is related to the unstable modes analyzed in [24, 34]. The decay term  $C_B$  is held very small relative to the growth rate for this simulation, and thus the effect of starvation due to the lack of nutrient is not readily apparent.

Figure 2 depicts the velocities around the biofilm hump for all three effective components at the mature stage. These velocities intuitively capture the motion of the bacteria, EPS and the solvent in the neighborhood of the nucleated hump. Specifically, the bacteria and EPS all expand in the bulge while the solvent expands near the top of the bulge and is replenished through the neck region. At the center of the nucleated hump, where the growth is the most significant, the bacterial and EPS velocity are near zero. The velocities show positive value indicating upward biomass expansion on top of the hump while they are negative in the lower half of the hump showing a downward expansion of the biomass. Due to the expansion of the biofilm front, the solvent is perturbed so that a pair of roll cells form on each side of the nucleated hump (Fig. 3). In this ternary model, the total volume of the mixture is assumed conserved, thus the growth of the bacteria and EPS is at the expense of the solvent. Figure 3 shows the velocity of the bulk fluid and the pressure field. The bulk velocity is the result of intermixing of the components which is dominated by the solvent velocity in this simulation. It is tiny however. The pressure is highest in the neck region and lowest behind the fast growing front. The relatively high pressure distribution shifts more toward the neck region as the biofilm growth approaches maturity. Overall, the pressure is quite low in magnitude.

Next, we investigate growth dynamics for differently sized biofilm colonies growing directly on the substrate. Figure 4 shows a simulation that initially has seven separate and disparately sized bacterial colonies. After 300 time units (about a half week of dimensional time) the biofilm has doubled in depth, and several colonies have grown together. The three colonies in the middle have begun connecting to each other at the top, leaving a void underneath and between with little EPS and bacteria. This suggests that, for the top feeding boundary condition, as the biofilm grows upward, the rate of outward expansion increases, especially at the spatial locations where the biofilm profile evolves along the dominating growth mode of certain wave numbers. This new growth forms nucleated regions that eventually converge to one another, and this growth profile is driven by the dominating unstable mode revealed from the linearized analysis [34]. Again, the

most populated bacterial and EPS regions are closer to the growing biofilm front. The decay term is held small in this case as well, but will be explored below.

The velocity of the three effective components are overlaid on the corresponding volume fraction plots in Figure 5. The roll cells are pushed upward as the biofilm fronts expand into the solvent region and merge. In the mature stage, only a pair of the roll cells survive on the top. Figure 6 shows snapshots of the velocity overlaid with the pressure field at two times for this multi-colony simulation. Early on, the velocity field undergoes a transient state before forming stable roll cells around each colony. The pressure and velocity here are still relatively small, which is expected given the very slow rate of growth associated with this biofilm.

When death due to a lack of nutrient is non-negligible, the dynamics of the growing biofilm are quite different. Figure 7 illustrates the effects of moderate cell death in a regime where the local nutrient concentration can become exhausted. Using the same initial condition as figure 1, figure 7 shows a significant departure from the usual mushroom shaped growth profile. Here we see much greater outward expansion of the bacteria, but lower local bacteria concentrations. Behind the fastest growing part of the biofilm, the bacteria populations decay to nearly zero, leaving pockets of little to no bacteria behind.

These studies demonstrate the basic hydrodynamics and reactive kinetics in biofilm growth among the three effective components.

## Remarks

- In these simulations the bacteria growth dynamics seem reasonable. The growth and decay rates of the biofilm along with the nutrient diffusion rate and relative distance from the upper, nutrient-rich, interface locally regulate the bacterial population.
- In each simulation we see rapid growth of the bacterial phase that tapers off as the local nutrient supply is exhausted. As the biofilm approaches maturity, we see cells near the bottom starved due to lack of available nutrient.
- The EPS growth lags slightly behind the growing bacterial front in these simulations. Since there is no mechanism to regulate EPS production in the current model, the EPS phase may continue to grow beyond realistic values given the presence of available nutrient. It is thought that bacterial EPS production is regulated through quorum sensing [2], and such a mechanism will be considered in an augmented model in the future.

We next probe how these growth dynamics and kinetics are altered when the biofilm is subject to a weak shear flow imposed by slow moving upper fluid layer.

## 2. *Growth in shear flows*

The disparity of time scales in the model suggests that some effects are negligible on the timescale where other effects are dominant. One example of this is that the elastic relaxation timescale of the EPS polymer ( $\lambda_1$ , usually in terms of seconds) is often small relative to the timescale under which biofilm growth occurs (usually over the course of hours and days). Likewise, under a large shear applied for a short time, the relative growth of the network will be small. Figure 8 demonstrates the effect of a biofilm growing under a weak shear where the Reynold's number for the solvent is  $Re_s = 1 \times 10^{-3}$  as calculated from the table of parameters. Here the shear is picked so small that its effects on growth can be seen only over the course of several days. Note that the growing biofilm under a weak shear can develop an elongated peninsula near the top of the biofilm hump, which can eventually pinch off and be carried away by the velocity field. Figure 9 records the snapshots of the pressure and the overlaid velocity field at two selected time values. Note that it is mostly bacteria along with the grafted EPS that are pulled off by the shear flow since the bacteria must proceed the EPS as the colony grows [45]. For mature biofilms, shedding bacteria is necessary for propagating the colony in other locations.

Under a relatively fast shear, where the characteristic time scale is set at  $t_0 = 1s$ , the timescale required to capture the growth effects is so small that the growth is negligible. Figure 10 shows a simulation of fast shear flow for a reasonably designed, heterogeneous biofilm profile with a slightly attenuated neck connected to a base, as suggest by Figure 4. In contrast to the weak shear experiments, where  $Re_s = 1 \times 10^{-3}$ , here the flow is actually three orders of magnitude faster, i.e.  $Re_s = 1$ . This is faster than the creeping flow experiments examined in figure 8, but still below the threshold for the onset of turbulence. Note that the biofilm bends under the influence of shear, but there is no visible growth. The shearing bulk flow induces consistent velocity in both the EPS and the bacteria (see Figure 11). The pressure distribution around the biofilm colony seems to indicate that the high pressure point is located in the neck region in the front of the hump, relative to the flow direction, and the low pressure spot is situated in the back of the hump (shown in Figure 12).

For heterogeneous biofilms, shear flow can be an important factor in propagation. Consider a mature biofilm grown using the same parameters as Figure 7. Most of the bacteria are densely

populated at the top of the biofilm, while a less dense population is spread throughout the network. If we apply a fast shear to this biofilm, as simulated in Figure 13, we see the less viscous bacteria at the top of the biofilm (where the EPS concentration is low), are quickly spread throughout the domain, while the bacteria near the base (where the EPS population is higher, and the velocity lower) remain intact. Thus, we can observe that the EPS network acts to hold the bacteria in place against shear flows.

## V. CONCLUSION

We have developed a multi-phase hydrodynamical theory for biofilms (biomass-solvent fluid mixtures) by modeling the EPS network, bacteria and effective solvent (consisting of solvent and all nutrient materials) explicitly. This theory is formulated using a single fluid multicomponent model of multiphase materials. In this model an incompressible average velocity field is prominently identified while the individual velocity for each fluid component is given as a combination of the (excessive) mixing velocity and the average velocity. The EPS dynamics are dictated by the local population of the bacteria and the presence of available nutrient. The bacterial population is affected by several factors including the local concentration of nutrient and the natural survival rate, which is modeled as a small decay rate independent of the environment. The nutrient concentration is governed by diffusion within the solvent and allows for local bacterial consumption. The governing system of equations for this model consist of partial differential equations for the volume fraction of each phase, the nutrient concentration, and the momentum transport equation for the mixture. These equations are discretized and solved numerically using second-order finite difference methods; the discrete equations are solved in 2-spatial dimensions in order to simulate biofilm growth and biomass-solvent interaction. Ranges of important parameter values are explored in order to demonstrate the features that this model is capable of capturing. The numerical simulations of biofilm growth in quiescent fluids reveal some prominent features for the spatial-temporal distribution of the bacteria and the EPS which we hope can be validated through refined experimental studies in the future. The numerical simulation tool also allows one to investigate the bacteria-EPS-flow interaction in shear flow environments as well as in environments where bacterial starvation, due to depletion of nutrient, may prevail. The theoretical framework we adopted in the development of this model can be readily extended to include different bacterial phenotypes, which are common in most biofilms, as well as antibacterial chemicals. These potentially

important refinements will be explored in a sequel.

This theoretical approach to multiphase complex fluids demonstrates a systematic derivation of the transport equations for volume fractions in an incompressible material system. Distinguishing the EPS and bacterial phases from one another allows for the differentiation of their production, transport, response to bulk flows, and mutual interaction. We note that previous models for biofilms did not treat differences in the physical properties of the bacteria and EPS in a systematic way. This modeling refinement is important, because it allows us to capture qualitative features of EPS and bacteria that emerge as a result of this distinction. As a more refined understanding of the EPS/bacteria relationship is developed, our model will further allow us to quantitatively address this issue. This approach also sets the stage for future studies on quorum sensing and additional chemical species transport, including the effects of flow and chemical interference on biofilm formation; it also enables the modeling of bacteria as an active migratory species within the modeling framework. All these applications will be pursued in the near future.

## **Acknowledgment**

Brandon Lindley and Qi Wang's research is partially supported by the National Science Foundation through grants DMS-0605029, DMS-0626180, EPS-0447660, DMS-0819051, DMS-0908330, and the International Cooperation and Exchanges Program of NSFC 10811120281 and NSFC grant 10601045. Tianyu Zhang's research is partially supported by the NSF grant DMS-0934696 and startup fund from Montana State University. Brandon Lindley acknowledges support from the National Research Council as a postdoctoral research associate at the U.S. Naval Research Laboratory.

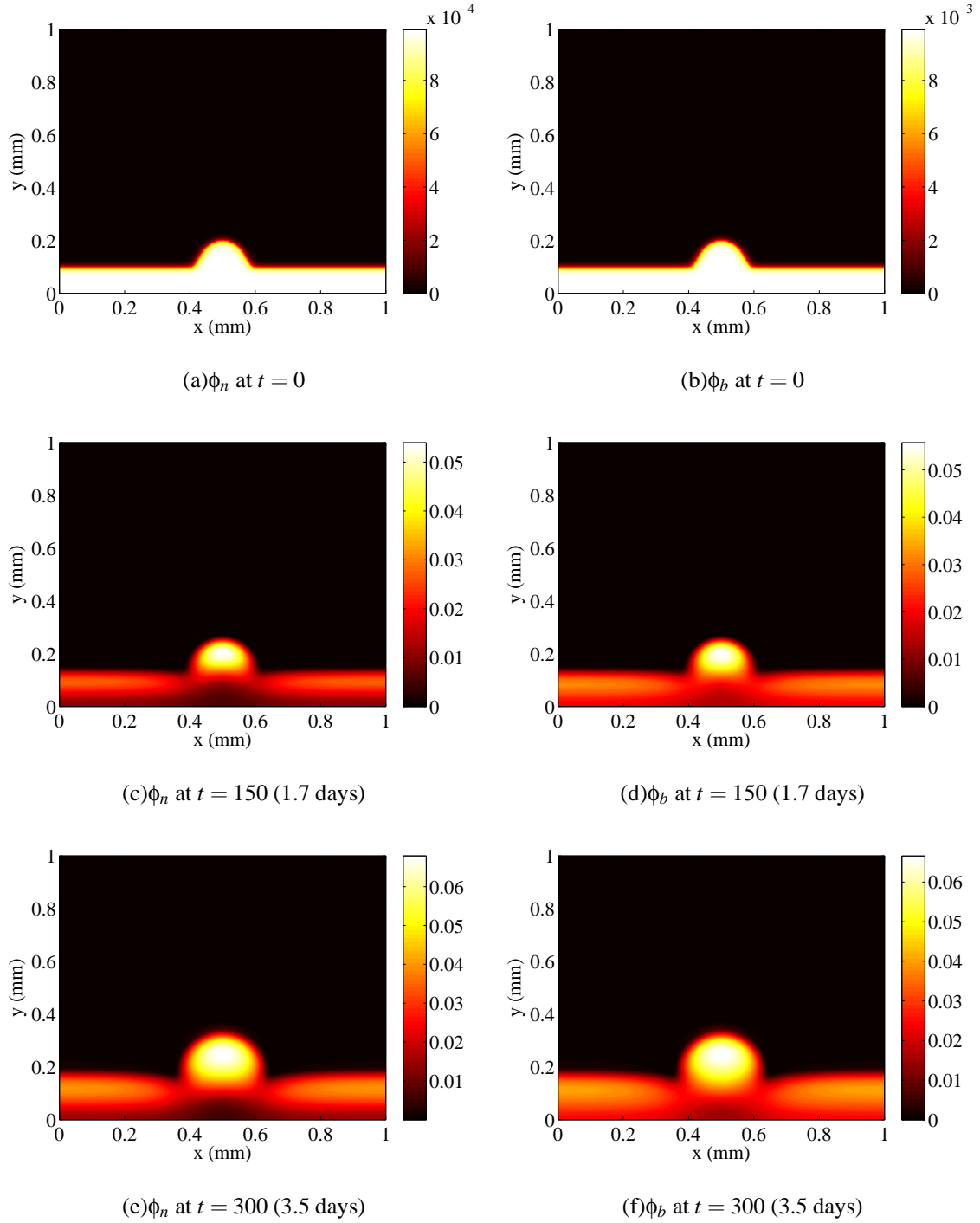


FIG. 1. (Color online) A growing biofilm forming a typical nucleated growth pattern. The volume fractions of  $\phi_n$  and  $\phi_b$  are shown at various timesteps, using parameters outlined in Table 1. The EPS volume fraction grows proportionally with that of the bacterial volume fraction.

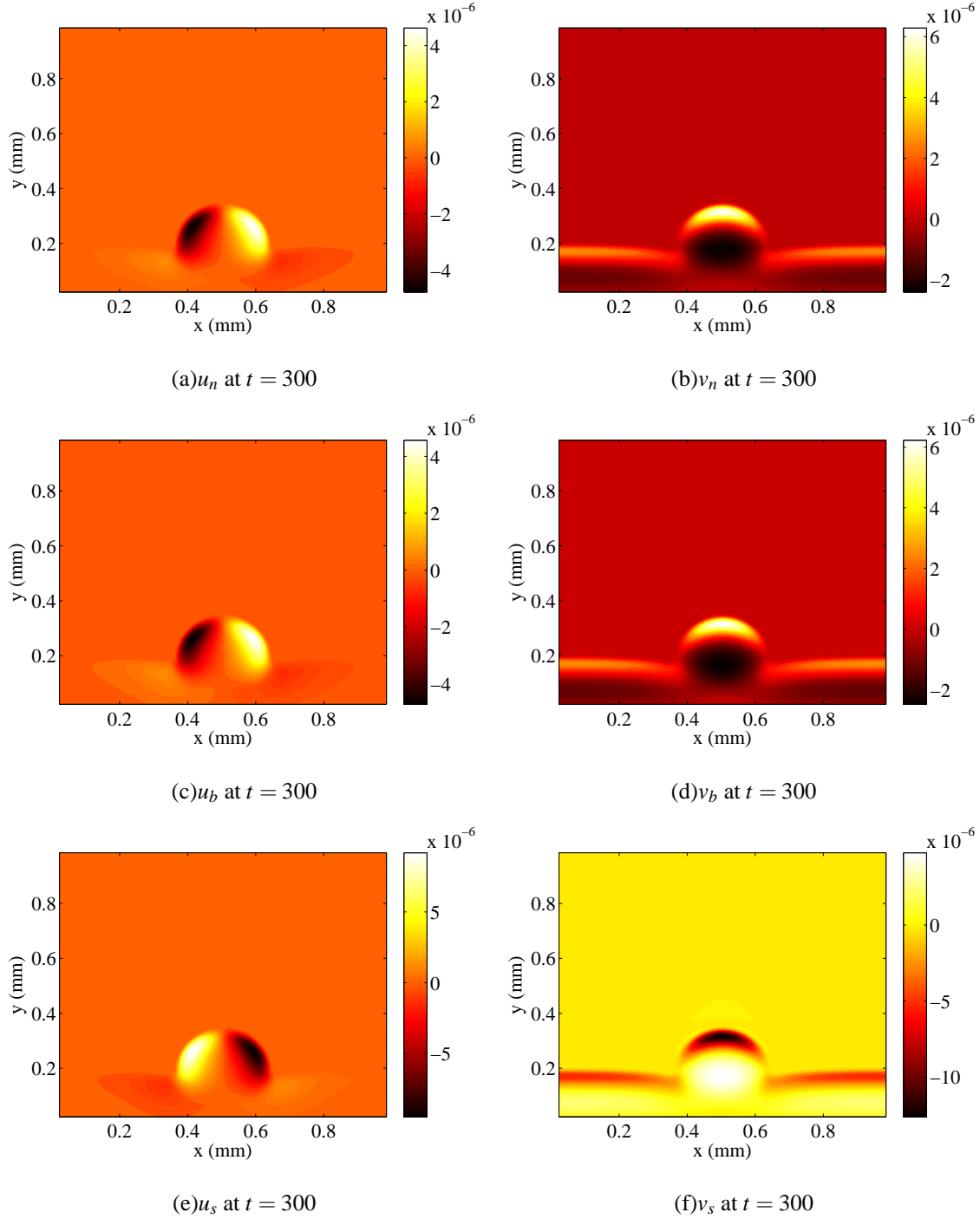


FIG. 2. (Color online) The  $x$  and  $y$  component of the velocity<sup>a</sup> for each phase in and around the growing biomass in Fig.1 at  $t = 300$ . Note that the direction field for the EPS and bacteria tend to move outward from the center of the nucleated hump, suggesting growth/expansion of the biofilm colony, while the solvent tends to replenish the interior of the biofilm through the neck region as well as within the biofilm. The solvent is pushed upward through the top of the hump leading to the formation of a pair of roll cells on each side of the bulging hump.

<sup>a</sup> Values of velocity or pressure shown in all figures are in the nondimensional units derived in equation III.1.

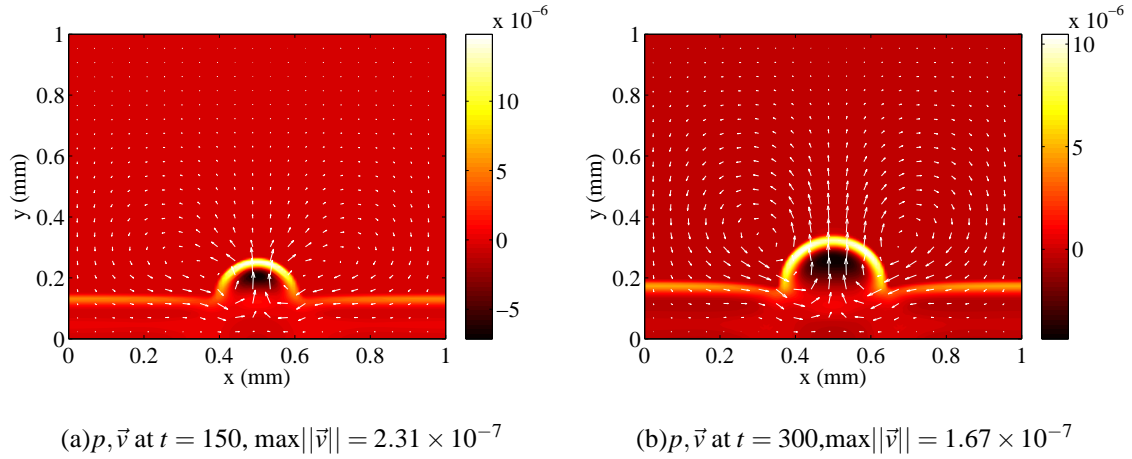


FIG. 3. (Color online) The bulk or average velocity field and pressure at  $t = 150, 300$  for the biofilm (of Fig.1), respectively. Here the direction field is overlaid with the pressure field (color map) at the corresponding timestep, and demonstrates the formation of roll cells (or vortices) in the solvent exterior to the growing biofilm.

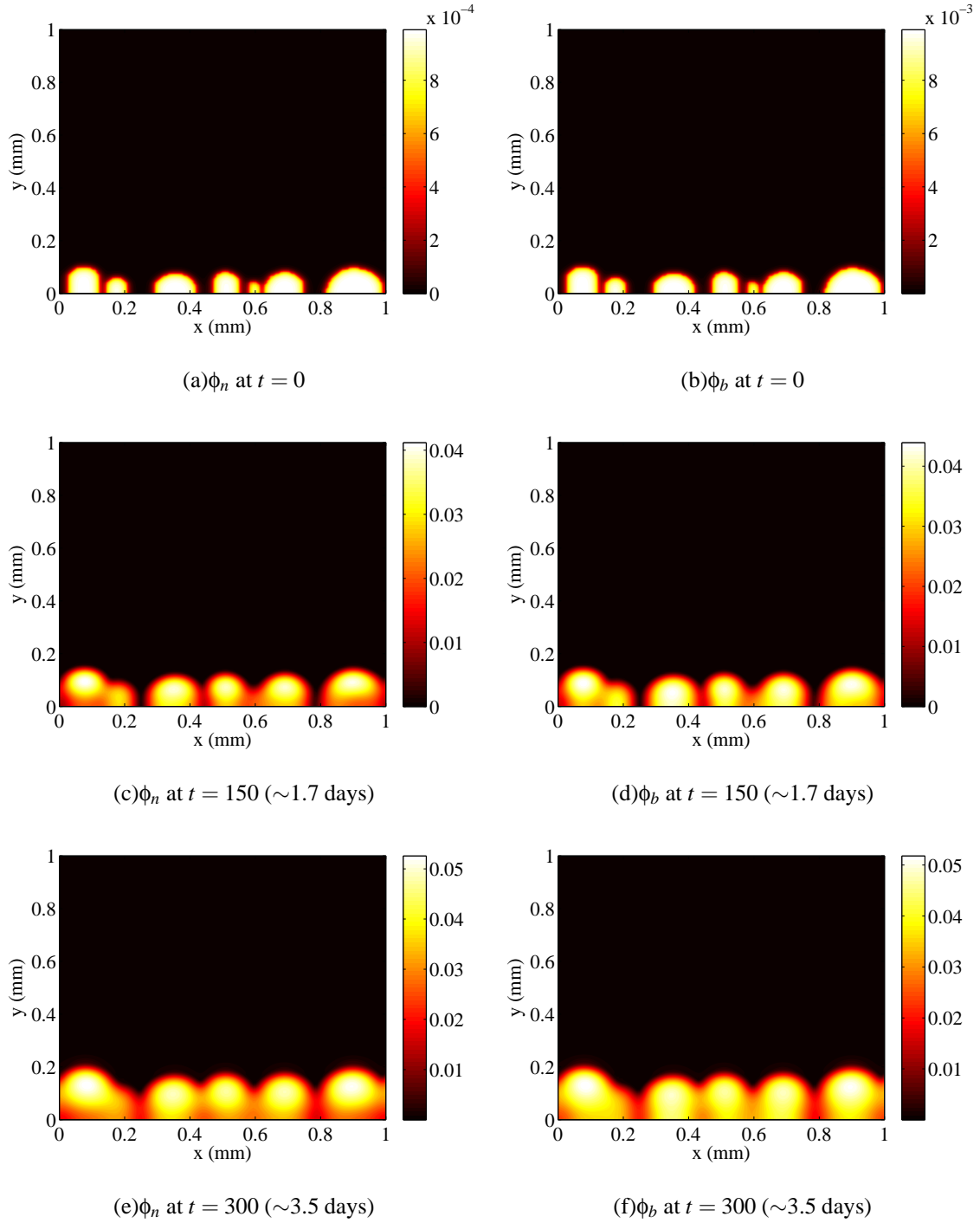


FIG. 4. (Color online) Disjoint biofilm colonies growing directly off a substrate. Here  $\phi_n$  and  $\phi_b$  are shown at various timesteps using the same parameter values listed in Table 1. As the biofilm colonies grow and merge together, heterogeneous structures in the EPS and bacteria profiles become evident.

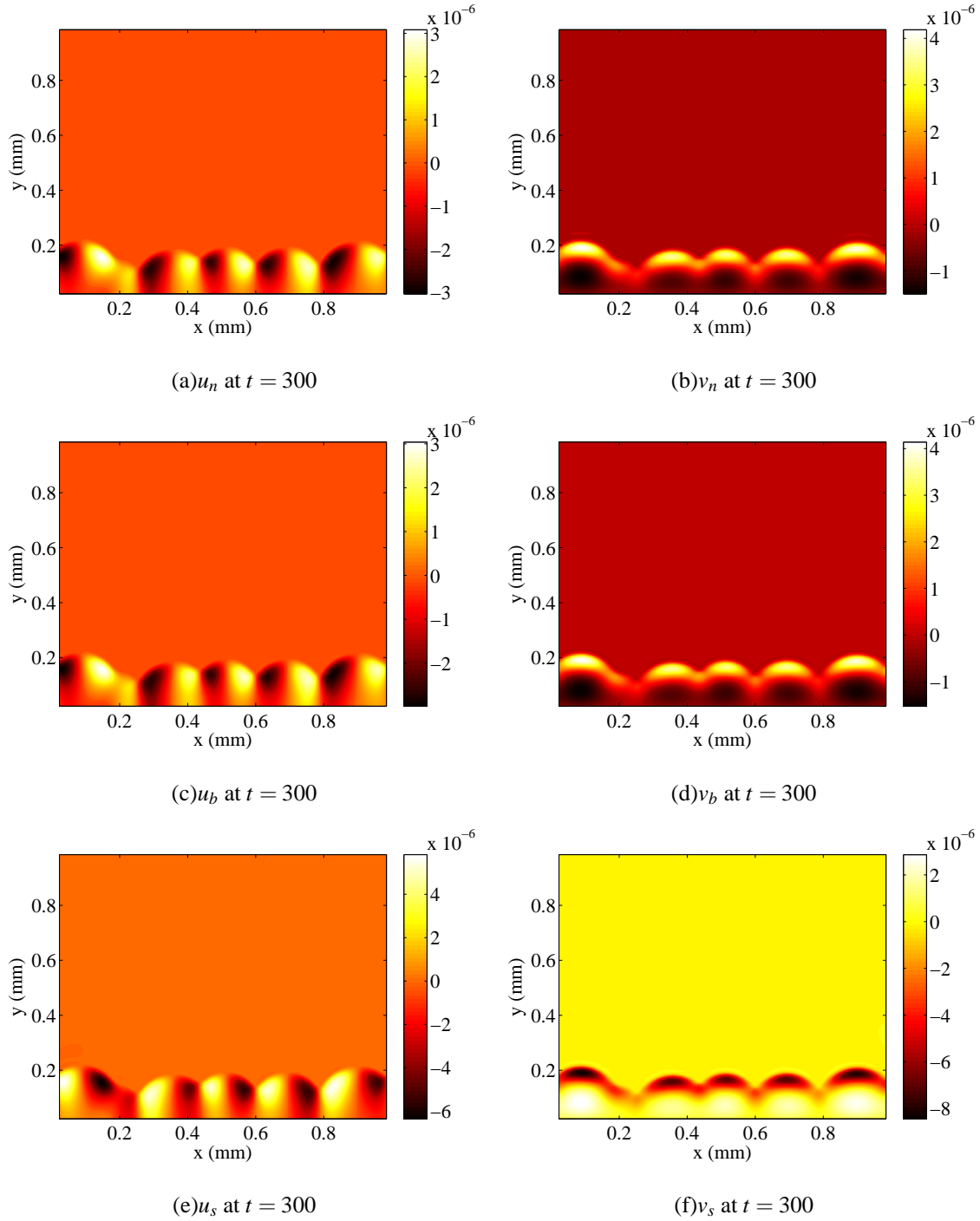


FIG. 5. (Color online) The velocity for each effective component around the growing colonies in Fig.4 at  $t = 300$ . Note that the direction field for the EPS and bacteria tend to move outward, suggesting growth of the biofilm colony, while the solvent tends to replenish the interior of the biofilm through the neck regions of the merging colonies as they expand outward. At the intermediate stage of growth, solvent tends to flow out the front of the nucleated region. A pair of roll cells form on the sides of each of the growing biofilm colonies.

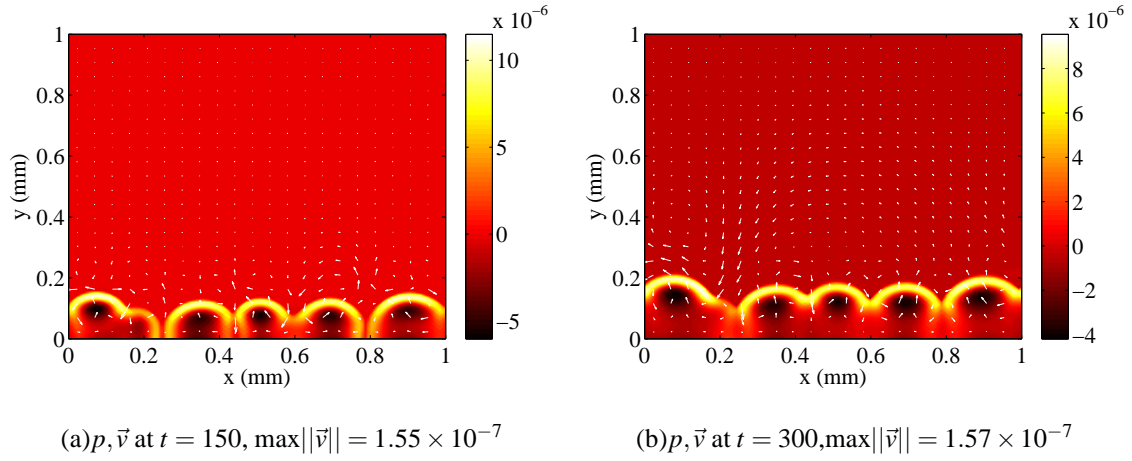


FIG. 6. (Color online) The bulk or average velocity field and pressure at  $t = 150, 300$  for the disjoint colonies of biofilm (of Fig.4). Here the direction field is overlaid with the pressure field (color map) at the corresponding timestep, and illustrates the formation of roll cells (or vortices) in the bulk fluid.

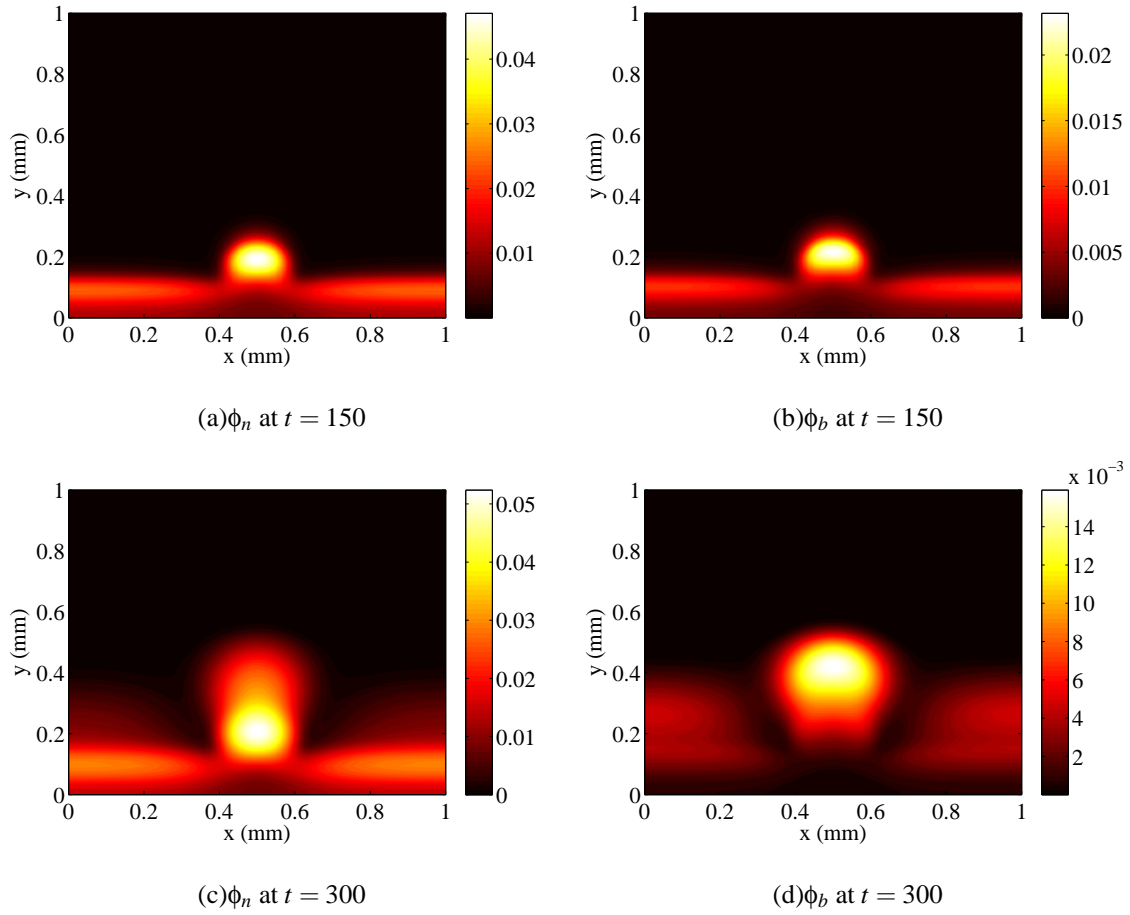


FIG. 7. (Color online) The growing hump of Figure 1 when starvation and natural cause decay is included in the model. Here a faster growth rate is used,  $\mu = 2.0 \times 10^{-4}$ , while the death rate is  $C_B = 2.0 \times 10^{-5}$ . Note that as the biomass grows, the oxygen content becomes diminished, and the bacteria tend to spread outward more in contrast to Figure 1. The EPS tends to form a long stalk trailing the upward expansion of the bacteria colony.

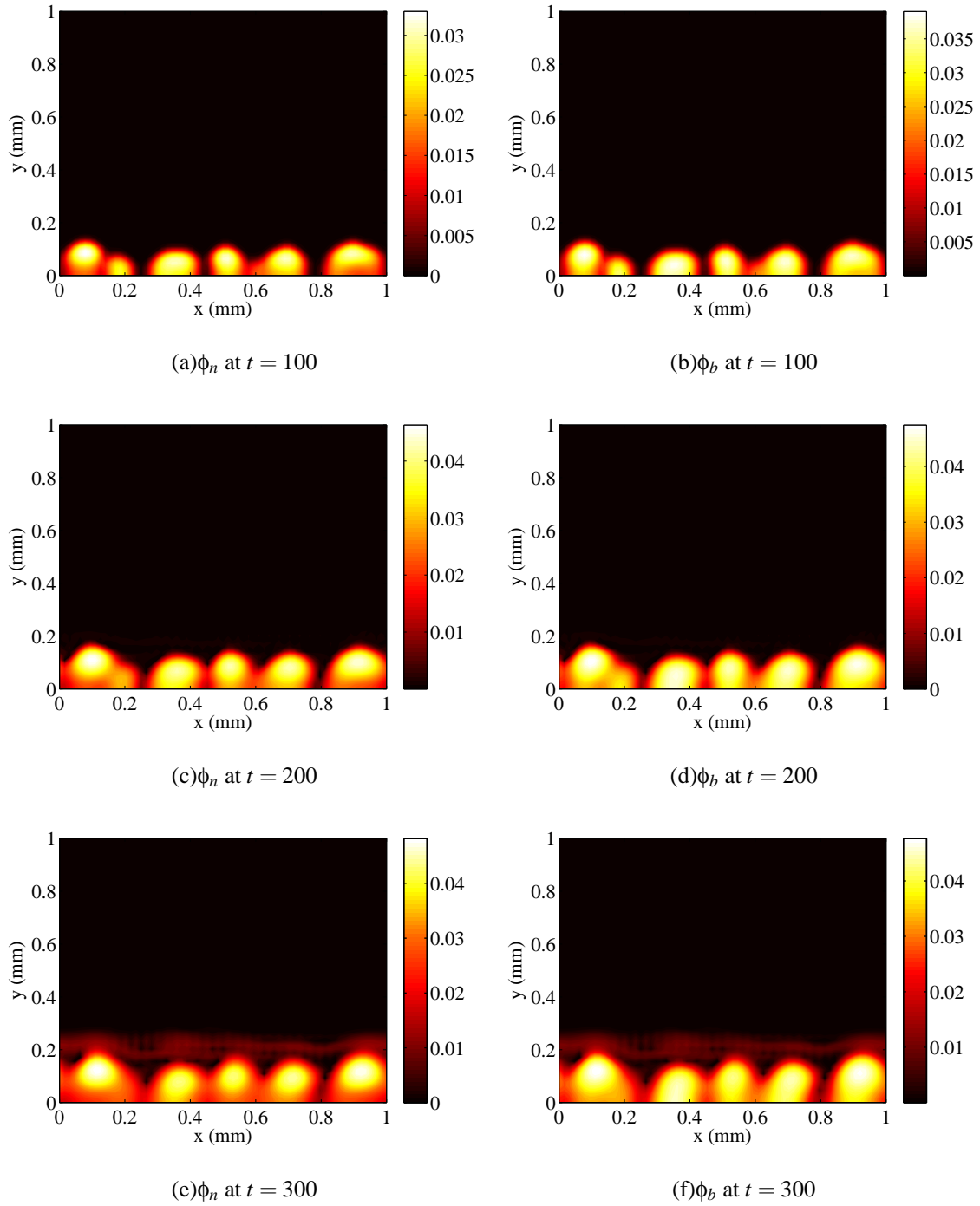


FIG. 8. (Color online) A growing biofilm under slow steady shear at  $t = 100, 200, 300$ . The biofilm is allowed to grow until  $t = 100$  before the shear flow is applied. Here the initial condition and parameters are the same as Fig.4 . The nondimensional shear rate of magnitude 1 is applied at  $y = 1$ . Shearing flow deforms the growing biofilm colony slightly to the flow direction, and begins pulling bacteria off the mature colony. The periodic boundary condition in the  $x$  direction is evident as we see streams of bacteria flow back in from the left side.

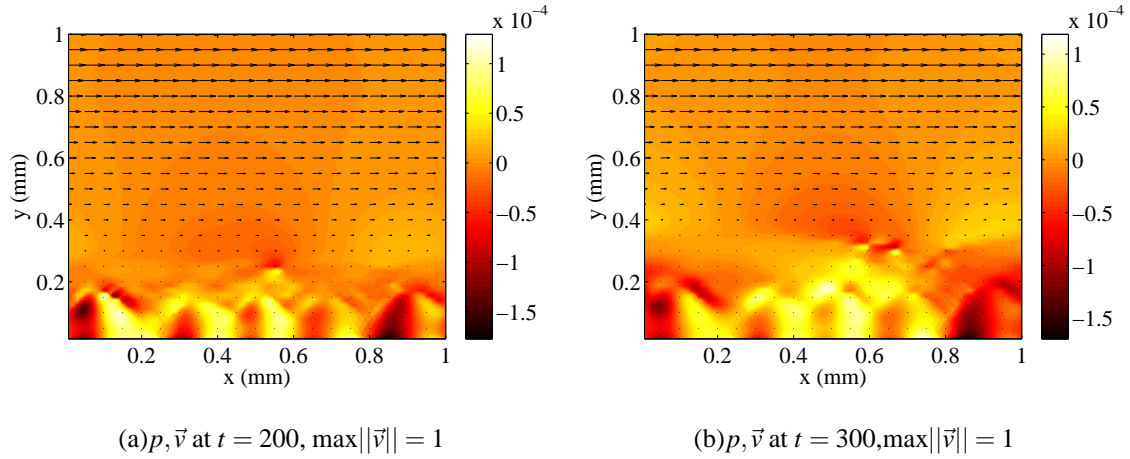


FIG. 9. (Color online) The bulk or average velocity field and pressure at  $t = 200, 300$  for the disjoint colonies of biofilm (of Fig.4) under slow steady shear. Here the velocity field is overlaid with the pressure field (color map) at the corresponding timestep and is depicted to illustrate the shear profile in the flow field.

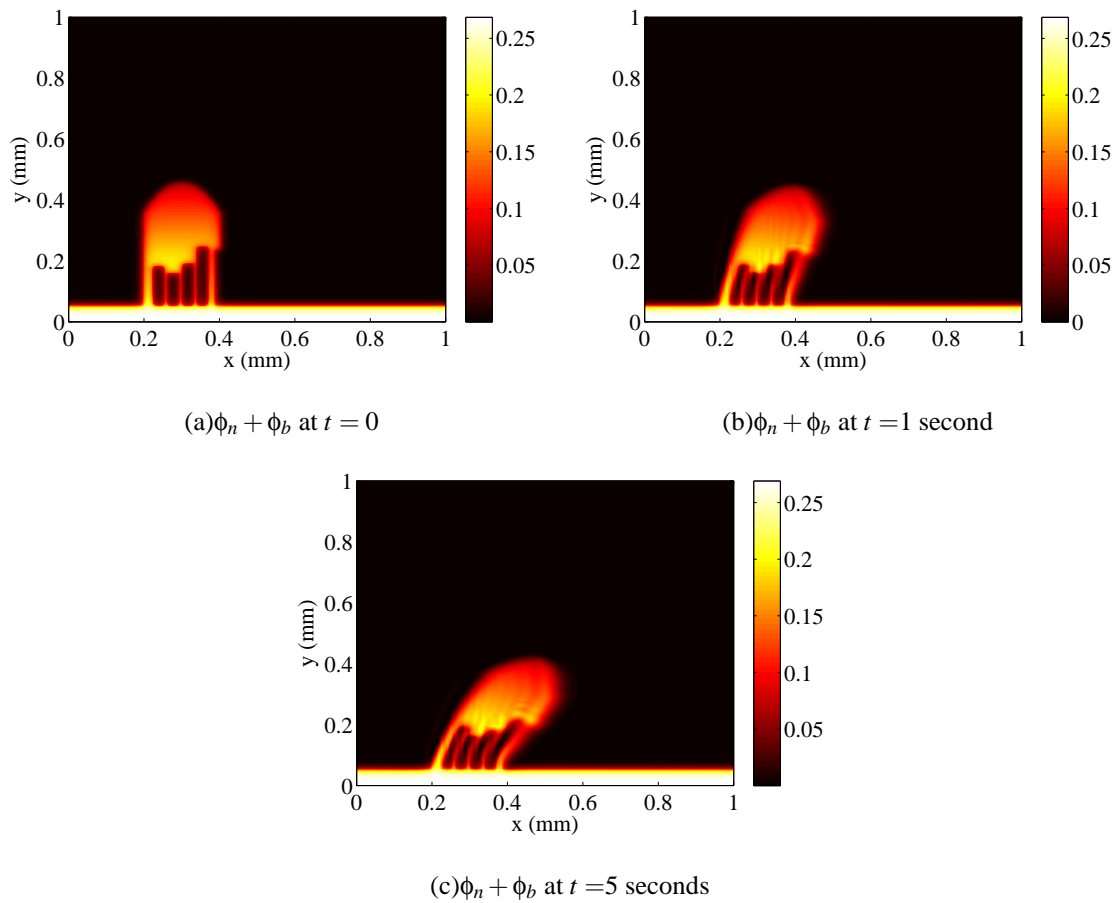


FIG. 10. (Color online) A heterogeneous biofilm growing on thin stalks under quick steady shear. The characteristic time scale here is  $t_0 = 1$ , and is picked to illustrate shear flow on the fast time scale. The nondimensional shear rate of magnitude 1 is applied at  $y = 1$ . Note that growth and mixing effect are negligible here and that the biofilm interface is well maintained.

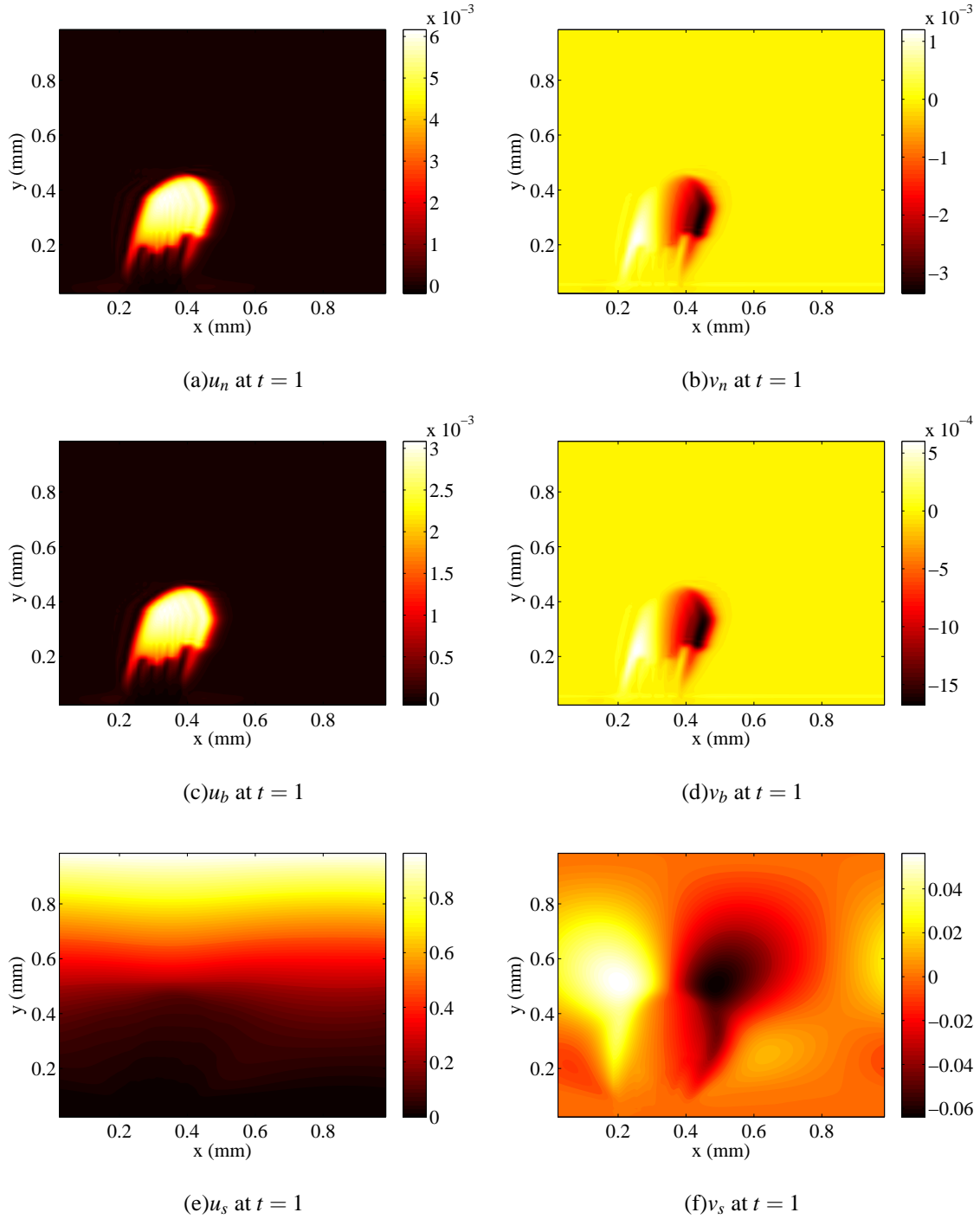


FIG. 11. (Color online) The velocity components in the quickly sheared biofilm. Here the same parameters are used as Fig.10, however bacterial growth and EPS relaxation are both neglected. The excessive velocity components indicate that the EPS and bacteria are moved to the right as the front of the hump is pulled upward and the back pushed down. The solvent velocity profile is typical for flow around an obstruction.

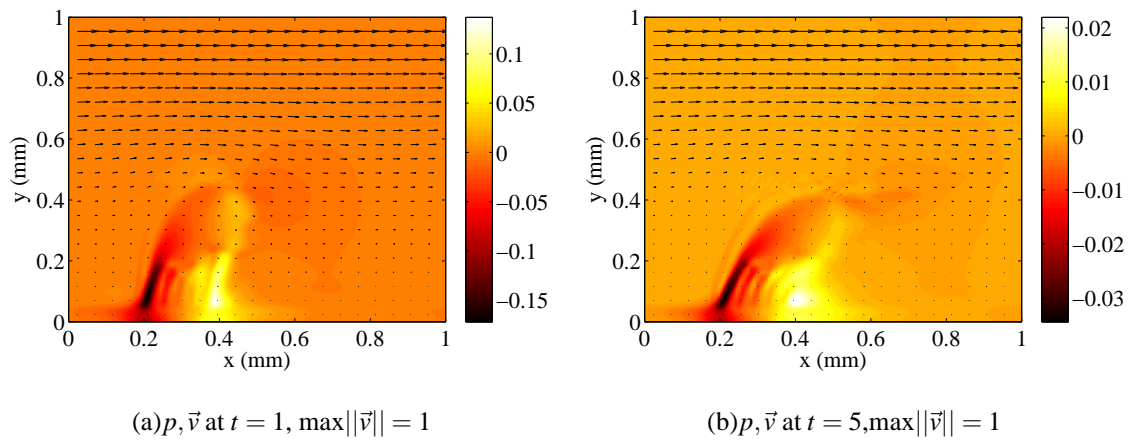


FIG. 12. (Color online) The average velocity field and pressure at  $t = 1, 5$ (seconds) for the quickly sheared biofilm (of Fig.10) . Here the direction field is overlaid with the pressure at the corresponding timestep, and is depicted to show the pressure jump from the leading edge to the back edge of the biofilm under shear.

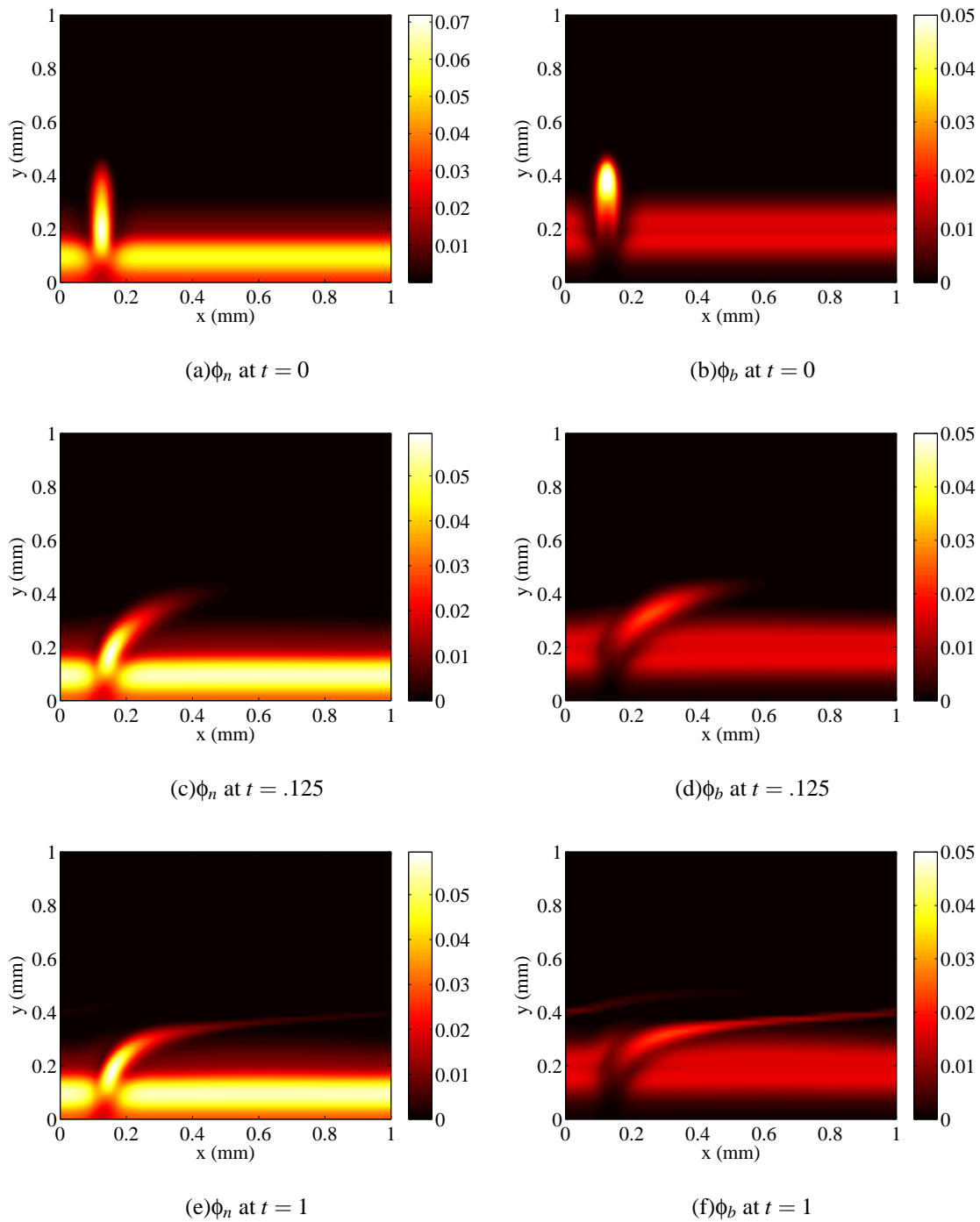


FIG. 13. (Color online) The mature biofilm from Figure 7 under fast steady shear. Like in Figure 10, the characteristic timescale is  $t_0 = 1$ . Here the shear rate is  $u = 10$  at the upper boundary  $y = 1$ , however. Note that the bacteria along with the attached EPS is prone to be pulled away into the solvent while the EPS network is more resistant to the applied shear.

- 
- [1] P. D. Leenheer and N. G. Cogan. Failure of antibiotic treatment in microbial populations. *arXiv*, 0807.1943v1, 2008.
- [2] M. R. Frederick, C. K. Kuttler, B. A. Hense, and H. J. Eberl. A mathematical model of quorum sensing regulated EPS production in biofilm communities. *Theoretical Biology and Medical Modelling*, 8(8):1-29, 2011.
- [3] B. E. Rittmann. The effect of shear stress on biofilm loss rate. *Biotech. Bioeng.*, 24:501–506, 1982.
- [4] B. E. Rittmann and P. L. McCarty. Evaluation of steady-state biofilm kinetics. *Biotech. Bioeng.*, 22:2359–2373, 1980.
- [5] B. E. Rittmann and P. L. McCarty. Model of steady-state-biofilm kinetics. *Biotech. Bioeng.*, 22:2243–2357, 1980.
- [6] O. Wanner and W. Gujer. Competition in biofilms. *Water Sci Technol.*, 17(2-3):27-44, 1985.
- [7] J. C. Kissel, P. L. McCarty, and R. L. Street. Numerical simulation of mixed-culture biofilm. *J. Environ. Eng.*, 110:393–411, 1984.
- [8] R. L. Colasanti. Cellular automata models of microbial colonies. *Binary Comput. Microbiol.*, 4:191, 1992.
- [9] G. C. Barker and M. J. Grimson. A cellular automaton model of microbial growth. *Binary Comput. Microbiol.*, 5:132–137, 1993.
- [10] J. W. T. Wimpenny, and R. Colstani. A unifying hypothesis for the structure of microbial biofilms based on cellular automaton models. *FEMS Microbiology Ecology*, 22(1):1-16, 1997.
- [11] D. R. Noguera G. Pizarro, D. Griffeath. Quantative cellular automaton model for biofilms. *J. Environ. Eng.*, 127:782–789, 2001.
- [12] G. Pizarro, R. Moreno C. Garcia, and M. E. Sepulveda. Two-dimensional cellular automaton model for mixed-culture biofilm. *Wat. Sci. Tech.*, 49:193–198, 2004.
- [13] E. Ben-Jacob, O. Schochet, A. Tenenbaum, I. Cohen, A. Czirok, and V. Tamas. Generic modelling of cooperative growth patterns in bacterial colonies. *Nature(London)*, 368:46–49, 1994.
- [14] S. W. Hermanowicz. A simple 2d biofilm model yields a variety of morphological features. *Math. Biosci.*, 169:1–14, 2001.
- [15] C. Picoreanu, M. C. Loosdrecht, and J. J. Heijnen. Discrete-differential modelling of biofilm structure. *Wat. Sci. Tech.*, 39(7):115–122, 1999.

- [16] C. Picoreanu, M. C. Loosdrecht, and J. J. Heijnen. Effect of diffusive and convective substrate transport on biofilm structure formation: a two-dimensional modeling study. *Biotech. Bioeng.*, 69:504–515, 2000.
- [17] C. Picoreanu, M. C. Loosdrecht, and J. J. Heijnen. Two-dimensional model of biofilm detachment caused by internal stress from liquid flow. *Biotech. Bioeng.*, 72:205–218, 2001.
- [18] C. Picoreanu, M. C. M. Loosdrecht, and J. J. Heijnen. A new combined differential-discrete cellular automaton approach for biofilm modeling: application for growth in gel beads. *Biotech. Bioeng.*, 57:718–731, 1998.
- [19] H. J. Eberl, D. F. Parker, and M. van Loosdrecht. A new deterministic spatio-temporal continuum model for biofilm development. *J. of Theor. Medicine*, 3(3):161–175, 2001.
- [20] H. J. Eberl and R. Sudarsan. Exposure of biofilms to slow flow fields. *J. of Theoretical Biology*, 253(4):788–807, 2008.
- [21] J. D. Dockery and I. Klapper. Finger formation in biofilm layers. *SIAM. J. Appl. Math.*, 62(3):853–869, 2001.
- [22] N. G. Cogan and J. P. Keener. The role of the biofilm matrix in structural development. *Math. Med. Biol.*, 21:147–166, 2004.
- [23] I. Klapper and J. Dockery. Role of cohesion in material description of biofilms. *Phys. Rev. E*, 74:031902, 2006.
- [24] T. Zhang, N. Cogan, and Q. Wang. Phase-field models for biofilms I. theory and simulations. *SIAM, J. Appl. Math.*, 69(3):641–669, 2008.
- [25] T. Zhang, N. Cogan, and Q. Wang. Phase-field models for biofilms II. 2-d numerical simulations of biofilm-flow interaction. *Commun. Comput. Phys.*, 4(1):72–101, 2008.
- [26] C. Chen, M. Ren, A. Srinivasan, and Qi Wang. 3-D simulations of biofilm-solvent interaction. *East Asian Journal on Applied Mathematics*, 1:197-214, 2011.
- [27] Q. Wang and T. Zhang. Mathematical models for biofilms. *Communication in Solid State Physics*, 150(21-22):1009–1022, 2010.
- [28] I. Klapper and J. Dockery. Mathematical description of microbial biofilms. *Siam Review*, 52(2):1–45, 2010.
- [29] I. W. Sutherland. The biofilm matrix - an immobilized but dynamic microbial environment. *Trends in Microbiology*, 9(5), 2001.
- [30] H. Horn, T.R. Neu, and M. Wulkow. Modeling the structure and function of extracellular polymeric

- substances in biofilms with new numerical techniques. *Wat. Sci and Tech.*, 43(6):121-127, 2001.
- [31] J. U. Kreft and J. W. T. Tempenny. Effects of EPS on biofilm structure and function as revealed by an individual-based model of biofilm growth. *Water Sci. and Tech.*, 43(6):135-141, 2001.
- [32] E. Alpkvist, C. Picoreanu, M. C. M. van Loosdrecht, and Anders Heyden. Three-dimensional biofilm model with individual cells and continuum EPS matrix. *Biotech. and Bioeng.*, 94(5):961-979, 2006.
- [33] K. Anguige, J. R. King, and J. P. Ward. A multi-phase mathematical model of quorum sensing in a maturing *Pseudomonas aeruginosa* biofilm. *Math. Biosci.*, 203:240-276, 2006.
- [34] B. Lindley, Q. Wang, and T. Zhang. A multicomponent model for biofilm-drug interaction. *Discrete and Continuous Dynamical Systems–Series B*, 15(2):417–456, 2011.
- [35] Q. Wang and T. Zhang. Kinetic theories for biofilms. *Discrete and Continuous Dynamical Systems: Series B*. 17(3):1027–1059, 2012.
- [36] J. N. Wilking, T. E. Angelini, A. Seminar, M. P. Brenner, and D. A. Weitz. Biofilms as complex fluids. *Materials Research Society Bulletin*, 36:385-391, 2011.
- [37] H. F. Winstanley, M. Chapwanya, M. J. McGuinness, and A. C. Fowler. A polymer-solvent model of biofilm growth. *Proceedings of the Royal Society A*, 467:1449-1467, 2011.
- [38] J. W. Cahn and J. E. Hilliard. Free energy of a nonuniform system. i: interfacial free energy. *J. Chem. Phys.*, 28:258–267, 1958.
- [39] J. W. Cahn and J. E. Hilliard. Free energy of a nonuniform system-iii: Nucleation in a 2-component incompressible fluid. *J. Chem. Phys.*, 31(3):688–699, 1959.
- [40] P. J. Flory. Thermodynamics of High Polymer Solutions. *J. of Chem. Phys*, 9(8):660, 1943.
- [41] J. Pyo and J. Shen. Gauge-Uzawa methods for incompressible flows with variable density. *Journal of Computational Physics*, 221, 181-197, 2007.
- [42] N. G. Cogan and J. P. Keener. Channel formation in gels. *SIAM J. Appl. Math.*, 65(6):1839-1854, 2005.
- [43] P. S. Stewart. Diffusion in biofilms. *J. Bacterio.*, 185(5):1485-1491, 2003.
- [44] I. Klapper, C. J. Rupp, R. Cargo, B. Purvedorj, and P. Stoodley. Visoelastic fluid description of bacterial biofilm material properties. *Biotech. Bioeng.*, 80:289-296.
- [45] Stoodley P, Cargo R, Rupp CJ, Wilson S, and Klapper I, "Biofilm material properties as related to shear-induced deformation and detachment phenomena," *J Industrial Microbiol Biotech*, 29(6):361-368, 2002.